FORSCHUNGSZENTRUM JÜLICH GmbH

Institut für Plasmaphysik
Association EURATOM-KFA

Comparison of the Code-Systems EB2-EIRENE and SAFE-EIRENE

Thomas Pütz

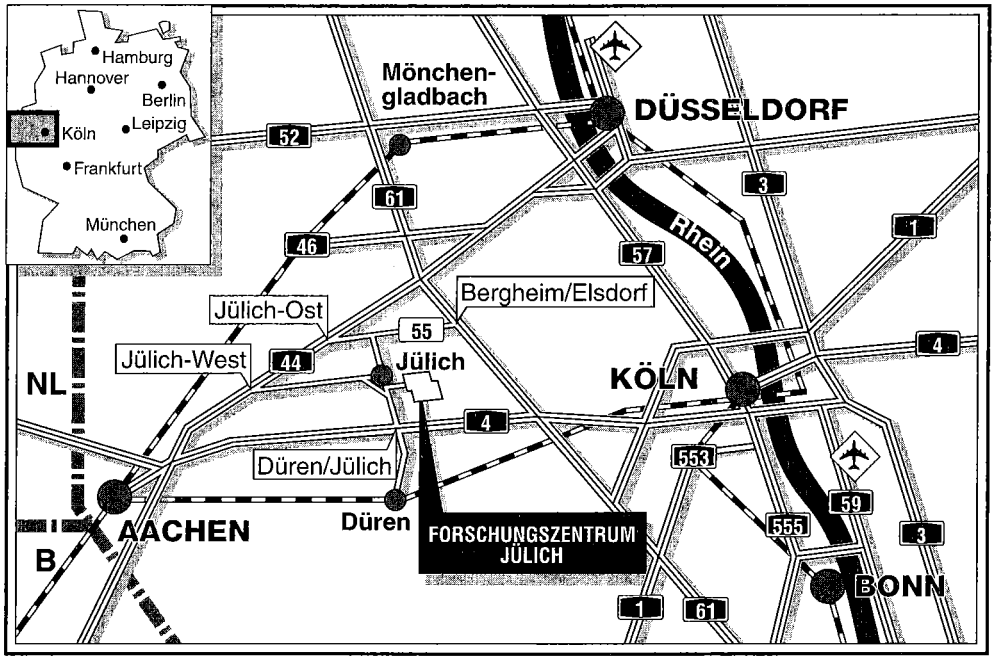

Berichte des Forschungszentrums Jülich ; 3220
ISSN 0944-2952
Institut für Plasmaphysik Jül-3220
Association EURATOM-KFA

Zu beziehen durch: Forschungszentrum Jülich GmbH · Zentralbibliothek
D-52425 Jülich · Bundesrepublik Deutschland
Telefon: 02461/61-6102 · Telefax: 02461/61-6103 · Telex: 833556-70 kfa d

Comparison of the Code-Systems EB2-EIRENE and SAFE-EIRENE

Thomas Pütz

Contents

Chapter 1

Introduction

A decisive question in plasma physics for nuclear fusion is how to extract from a TOKAMAK device the large amounts of energy and alpha particles produced in the core plasma? Since these fluxes are mainly controlled by the plasma edge several magnetic configurations and geometrical features are proposed for this region.
Until now in all concepts a system with a plasma-surface interface (target) is used to control the fluxes of particles and energy. The system has to be designed and optimized to meet different requirements:

- It should handle the intense, hot plasma exhaust, while the power density on the targets must stay below technological limits.
- The interference with the high temperature core plasma should be not too strong to sustain the fusion reactions.
- The system has to guarantee a sufficiently good particle exhaust, to remove the α-particles out of the core.

In general, current experiments cannot be scaled to future devices, due to the lack of appropriate similarity parameters. Therefore model calculations of the plasma edge are necessary to optimize core conditions and to control heat and particle exhaust. In addition to that changes in the models may help to understand the behaviour of the plasma edge.

First theoretical considerations started with simple 1-dimensional calculations, either modelling the radial transport or the transport along field lines. But in most experiments the fluxes in radial direction and parallel to the field are strongly coupled. Beginning with nearly pure diffusion across magnetic surfaces inside the separatrix the direction of the flow changes and in the region, where field lines intersect a material boundary (**S**crape **O**ff **L**ayer) the flow along field lines becomes comparable to the diffusion. This spatially localized contact with the targets combined with the strong gradients in plasma density and temperature ($\| \vec{B}$ and $\perp \vec{B}$) makes it unavoidable to use at least two-dimesional models. Moreover the various and complex interactions of the plasma with neutral particles or impurities generated at the targets has to be taken into account. One rapidly reaches a level of complication and of strong and nonlinear mutual dependence of the variables that a solution of the transport equations is only

possible using numerical methods.

Over the last years two dimensional plasma edge transport codes, combined with physically detailed Monte Carlo models for the neutral particles have become a common tool to investigate tokamak edge physics. Complementary to the most widely used finite volume methods we developed a code based on a finite element technique. In this report our experience with this code is summarized and the results obtained with the different numerical methods are compared.

The paper is organized as follows:

- **Chapter 2:** The commonly used fluid equations, the typical geometry and the characteristic boundary conditions are presented. From these model equations fundamental transport processes are isolated giving first indications for appropriate numerical schemes, which should be used to get physically meaningful solutions.

- **Chapter 3:** An overview of the numerical methods is given, which are used to solve convection-conduction equations. Starting from a general formulation, the relation between the finite volume method (FVM) and the finite element method (FEM) is explained. Furthermore it is shown in which way both schemes can take into account the special properties of the equations modelling the plasma flow. This will be discussed with special reference to the finite volume code B2 and the finite element code SAFE.

- **Chapter 4:** The coupling of the finite element code SAFE to various source term models is described. These models are needed to comprise the interactions of the plasma with neutral particles generated at the target plates. We will refer to both a simple analytical model especially developed for triangular meshes and the physically more realistic but computational more demanding Monte-Carlo-model of EIRENE.

- **Chapter 5:** Results of calculations with the SAFE-EIRENE code and the B2-EIRENE code are compared. Therefore we have used the same geometry, the same transport coefficients and boundary conditions and a nearly equal degree of spatial resolution. The correlation between the different results of the two codes and the different numerical treatment is elucidated.

- **Chapter 6:** Conclusions are drawn leading to suggestions for a hybrid code, which take advantage of the positive aspects of both methods. Finally we give an outlook on how such a code can be organized.

Chapter 2

2-D Modelling of the Plasma Edge

2.1 The model equations

In a magnetized plasma the charged particles are constrained -in lowest approximation- to follow the twisted magnetic field lines. For this high field case Braginskij has formulated fluid model equations using general co-ordinate free tensor notation. Starting from these equations and assuming toroidal axisymmetry -as the geometry of a TOKAMAK is- a two-dimensional edge model has been derived [1, 2] describing the plasma parameters in one poloidal cross section of the torus. Within the flux surfaces, the "classical" transport equations are retained. A major change is the "ad-hoc" introduced Diffusion Ansatz for the radial transport, due to experimentally observed "anomalous" particle and energy flux perpendicular to the magnetic surfaces. Furthermore the plasma is considered to be quasineutral; electric currents and diamagnetic drifts are neglected.
These modifications lead to a reduced set of two-dimensional fluid equations in the poloidal-radial plane (x_θ, r). It consists of a continuity equation governing the ion density n_i, a momentum balance equation governing the poloidal flow velocity u and equations of the Navier-Stokes form governing the electron- and ion temperatures T_e and T_i. In addition to that the radial velocity v is determined by a simple diffusion equation. Auxiliary variables are the mass density $\rho = m_i n_i$, the electron and ion pressures, $p_e = n_e T_e$ and $p_i = n_i T_i$, the total pressure $p = p_e + p_i$ and the kinetic energy of the ions $\frac{1}{2}\rho w^2 = \frac{1}{2}\rho\{(\frac{u}{b_\theta})^2 + v^2\}$, where $b_\theta = \frac{B_\theta}{B}$ is the ratio of the poloidal magnetic field to the total field strength.
The continuity equation, the equation for poloidal momentum and the equations for ion and electron energy can be written in convection-conduction form. For simplification we omit metric coefficients (The complete system is given elsewhere, see e.g. [1]) and thereby get the formula:

$$\frac{\partial}{\partial t}\vec{U} + \frac{\partial}{\partial x_\theta}\vec{F} + \frac{\partial}{\partial r}\vec{G} = S \tag{2.1}$$

where the vector $\vec{U}$ contains only "conservative" variables:

$$\vec{U} = \begin{pmatrix} \rho \\ \rho u \\ \frac{3}{2}p_i + \frac{1}{2}\rho w^2 \\ \frac{3}{2}p_e \end{pmatrix} \tag{2.2}$$

The vectors $\vec{F}$ and $\vec{G}$ are decomposed into a purely convective and a remaining part with conductive contributions:

$$\vec{F} = u \cdot \vec{U} + \begin{pmatrix} 0 & & \\ & -\eta_\theta \frac{\partial u}{\partial x_\theta} & \\ up_i & -u\frac{\eta_\theta}{b_\theta^2}\frac{\partial u}{\partial x_\theta} & -\kappa_\theta^i \frac{\partial T_i}{\partial x_\theta} \\ up_e & & -\kappa_\theta^e \frac{\partial T_e}{\partial x_\theta} \end{pmatrix} \tag{2.3}$$

$$\vec{G} = v \cdot \vec{U} + \begin{pmatrix} 0 & & \\ & -\eta_r \frac{\partial u}{\partial r} & \\ vp_i & -u\frac{\eta_r}{b_\theta^2}\frac{\partial u}{\partial r} & -\kappa_r^i \frac{\partial T_i}{\partial r} \\ vp_e & & -\kappa_r^e \frac{\partial T_e}{\partial r} \end{pmatrix} \tag{2.4}$$

The vector $\vec{S}$ includes all source terms and external forces:

$$\vec{S} = \begin{pmatrix} S_n & & \\ b_\theta S_m & -b_\theta^2 \frac{\partial p}{\partial x} & \\ S_{Ei} & -u\frac{\partial p_e}{\partial x_\theta} & +c_{equi}(T_e - T_i) \\ S_{Ee} & +u\frac{\partial p_e}{\partial x_\theta} & -c_{equi}(T_e - T_i) - P_{rad} \end{pmatrix} \tag{2.5}$$

In addition to that we have the equation for the radial momentum

$$\rho v = -D \cdot \frac{\partial \rho}{\partial r} \tag{2.6}$$

The terms S_n, S_m, S_{Ei} and S_{Ee} are volume sources of particles, momentum, electron and ion energy. Separately defined is the loss of electron energy P_{rad} due to radiation, mainly caused by the interactions with impurities. The factors η_θ and η_r are the poloidal and radial ion viscosity coefficients, $\kappa_\theta^{i,e}$ and $\kappa_r^{i,e}$ are the poloidal and radial thermal conductivities, $c_{equi}(T_e - T_i)$ is a temperature equilibration term and D is the "anomalous" radial diffusion coefficient.

The transport coefficients are strongly nonlinear functions of the variables ($\eta_x^{i,e} \sim T_{i,e}^{5/2}; \kappa_\theta^{i,e} \sim T_{i,e}^{5/2}; c_{equi} \sim n \cdot T_e^{-3/2}$) and their relative magnitude varies in radial direction by several orders of magnitude. In poloidal/parallel direction the variation is usually less than a factor of ten and one can estimate which part of the momentum and energy flux is due to convection and conduction respectively (see discussion below).
The source terms are associated with exchange of momentum and energy between plasma electrons and ions or with interaction of the plasma with neutral particles (ionization, charge exchange, recombination, radiation). The contribution from the neutrals has a complicated nonlinear and non-local dependence on the unknows.
However, in general the electron energy transport ($\|\vec{B}$) is much faster than the ion

energy transport ($\| \vec{B}$) and the radial diffusion ($\perp \vec{B}$) is much slower than parallel transport. From such crude arguments one can get estimates for the typical decay lengths in radial and in poloidal/parallel direction. The ratio of these lengths is approximately similar to the geometric length scales of the plasma edge. It has a radial extension of about 0.1 m and a poloidal (parallel) length in the order of 1 m (10 m).

2.2 The boundary conditions

To solve the differential equations mentioned above, one has to specify an appropriate number of values for the unknowns and/or their derivatives at the boundary of the geometrical domain. A mathematically correct way to determine the boundary conditions required is to find the characteristics of the equations (eigenvalues and eigenvectors). Then the right number of boundary conditions for the new variables (eigenvalues) at the right surfaces (perpendicular to the eigenvectors) is given by the order of the differential equation along each characteristic direction (parallel to the eigenvectors). Because of the strong nonlinearities the usual (linearized) procedure to find these characteristics is not applicable here. Therefore we use a simple approximation, partly justified by the strong anisotropy in transport: The derivatives in each direction ($\| \vec{B}$;$\perp \vec{B}$) are counted. One sees, that seven boundary conditions are needed at the boundaries normal to the poloidal/parallel coordinate, and that eight conditions are required at boundaries perpendicular to radial coordinate.
For the two energy equations one has to specify either the energy fluxes or the temperatures (or more generally a combination of both) on each segment of the boundary (two segments $\perp \vec{B}$; $\perp x_\theta$, two segments $\| \vec{B}$; $\perp r$). For the poloidal momentum equation one usually imposes a sonic flow parallel to the field lines on one segment ($\perp x_\theta$) and zero flow or zero shear elsewhere. To determine the number of boundary conditions for the density, the equation for the radial transport is inserted into the continuity equation. Thereby one gets an equation of second order in radial direction and hence the need for two conditions. e.g. one on each face ($\perp$ r). In poloidal direction only one condition, determining either the density itself or the particle flux, is required.

2.3 Basic transport processes

In this section characteristic times for basic transport processes in the plasma edge are derived heuristically. For each of these relaxation times we assume only one physical effect to be dominant. Moreover the differential operators are replaced by typical gradient lengths measured in the SOL of TEXTOR.
Although the plasma parameters in other devices may differ by a factor of ≈ 2 this approximation shows some general features of the transport described by the model equations.

The radial diffusive transport All radial transport coefficients are chosen empirically, but their physical interrelation is retained. Thus each physical quantity is transported purely diffusive and the relaxation times for particle-, momentum- and

energy-transport perpendicular to the magnetic field are nearly the same. Assuming a typical radial gradient length of about $\Delta r_n \approx 2cm$ in the SOL and a diffusion coefficient of about $D \approx 0.5m^2/s$ we find a characteristic relaxation time of:

$$\tau^{D,rad} = \frac{(\Delta r_n)^2}{2D} \approx 5 \cdot 10^{-4} s \tag{2.7}$$

The parallel convective transport and the propagation of sound waves The characteristic timescales for these transport processes can be obtained by solving simultaneously continuity-, momentum- and energy-balance in parallel/poloidal direction, neglecting dissipative terms (adiabatic approach). Defining the sound velocity $C_S = \sqrt{5/3 \cdot (T_i + T_e)/m_i}$ and using the velocity (pressure) gradient length in parallel direction $[\Delta L_{||}]_V$ ($[\Delta L_{||}]_P$) typical relaxation times are approximately:
(temperatures approximately 15 eV; $(\Delta L_{||})_V \approx 4m$; $(\Delta L_{||})_P \approx 2m$)

$$\tau_{ion}^{conv,||} = \frac{(\Delta L_{||})_V}{V_{||}} \approx \begin{cases} 1 \cdot 10^{-4} s & : \ at\ the\ target \ \ (V_{||} = \sqrt{(T_i + T_e)/m_i}) \\ 1 \cdot 10^{-1} s & : \ at\ the\ symmetry\ plane \ \ (V_{||} \approx V_r) \end{cases} \tag{2.8}$$

$$\tau_{ion}^{sound,||} = \frac{(\Delta L_{||})_P}{C_S} \approx 5 \cdot 10^{-5} s \tag{2.9}$$

The parallel dissipative momentum transport The dissipative momentum transport is generated by viscosity effects. The corresponding relaxation time results in:

$$\tau_{ion}^{\eta,||} \approx \frac{3 n_i m_i}{8 \eta_{||}} \cdot (\Delta L_{||})_V^2 \approx 5 \cdot 10^{-5} s \tag{2.10}$$

The parallel heat conduction of the ions This transport process is connected to the dissipative momentum transport via the relation:

$$\kappa_{||} = \frac{4.06 \cdot \eta_{||}}{m_i} \tag{2.11}$$

with a relaxation time of:

$$\tau_{ion}^{\kappa,||} = \frac{3 n_i}{4 \kappa_{||}} \cdot (\Delta L_{||})_T^2 \approx \frac{1}{8} \tau_{transp}^{\eta,||} \approx 6 \cdot 10^{-6} s \tag{2.12}$$

The poloidal heat conduction of the electrons The electron heat conduction is the process with the shortest relaxation time, because the transport coefficient is by a factor of $\sqrt{m_{ion}/m_e}$ larger than the one for the ions. Thus for a pure deuterium plasma:

$$\tau_{el}^{\kappa,||} \approx \frac{1}{60} \tau_{ion}^{\kappa,||} \approx 1 \cdot 10^{-7} s \tag{2.13}$$

The relation between these times can be used to adapt the numerical treatment to the physical problem and to facilitate an interpretation of the numerical solution.

2.4 Requirements for the numerical solution procedure

The relation between different timescales derived from the model equations in the last section elucidates various aspects of the underlying physics which have to be reflected in an appropriate numerical treatment.

2.4.1 Transport along field lines

1. **Introduction of flux limits**
   On one hand the ratios between the relaxation times for conductive transport and for sound propagation $\tau_{ion}^{\eta,\|}/\tau_{ion}^{sound,\|}$ (momentum), $\tau_{ion}^{\kappa,\|}/\tau_{ion}^{sound,\|}$ (energy) can be determined using the values calculated above:

$$\frac{\tau_{ion}^{\kappa,\|}}{\tau_{ion}^{sound,\|}} \ll \frac{\tau_{ion}^{\eta,\|}}{\tau_{ion}^{sound,\|}} \approx 1 \tag{2.14}$$

   On the other hand one finds by inserting the expression for $\eta_\|$ into the formula for $\tau_{ion}^{\eta,\|}$:

$$\frac{\tau_{ion}^{\eta,\|}}{\tau_{ion}^{sound,\|}} = 1.1 \cdot \frac{(\Delta L_\|)_V}{\lambda_{mfp}} \gg 1 \tag{2.15}$$

   ($\lambda_{mfp} \ll (\Delta L_\|)_V$ has to be fulfilled for the fluid approach to be valid)
   To remedy this contradiction the easiest way - not in any case meaningful - is to define a "flux limit". Thereby the conductive flux is restricted to a certain fraction of the collision-free flux, which is the physically maximal value generated through pressure gradients. The flux limit is applicable for both the momentum and the ion energy equation.
   In the same way a flux limit for the electron energy equation can be defined where the upper limit is the energy transport with the electron thermal velocity.

2. **Reynolds-number, Peclet-number**
   We consider a simple one dimensional convection-conduction equation of the form

$$\frac{\partial(\rho\Phi)}{\partial t} + \frac{\partial(\rho u \cdot \Phi)}{\partial x} = \frac{\partial}{\partial x}\left(\chi \frac{\partial \Phi}{\partial x}\right) \tag{2.16}$$

   with boundary conditions $\Phi(0) = \Phi_0$ and $\Phi(L) = \Phi_L$. Within a short interval, which can be identified as a cell length in our discretized geometry a constant transport coefficient χ can be assumed and hence one finds the stationary solution [4]:

$$\Phi = \Phi_L \cdot \frac{e^{Z\frac{x}{L}} - 1}{e^Z - 1} - \Phi_0 \cdot \frac{e^{Z\frac{x}{L}} - e^Z}{e^Z - 1} \tag{2.17}$$

   with the characteristic number $Z = \frac{\rho u L}{\chi}$.
   For $Z \gg 1$ the transport is dominated by convection, for $Z \ll 1$ it is dominated

by conduction. In fluid mechanics Z is called the Reynolds-number $Re = \frac{\rho u L}{\eta}$ for momentum flow ($\Phi = \rho u$) and the Peclet-number $Pe = \frac{\rho u L}{\kappa}$ for energy flow ($\Phi = T$).
These numbers are related to the characteristic timescales:

$$Re = \frac{\tau_{ion}^{\eta,\|}}{\tau_{ion}^{conv,\|}} \quad and \quad Pe = \frac{\tau_{ion}^{\kappa,\|}}{\tau_{ion}^{conv,\|}} \tag{2.18}$$

and vary between $10^{-3} - 10^{-4}$ (purely conductive) at the symmetry plane and $1 - 100$ (more or less convection dominated depending on the flux limit) at the target. Because their values strongly affect the solution, the numerical scheme used to solve the transport equations should be able to handle both cases, strong conduction and strong convection.

3. **Energy transport for ions and electrons ($\|\vec{B}$)**
   As stated above the energy relaxation $\|\vec{B}$ for electrons is much faster than for ions:

$$\frac{\tau_{ion}^{\kappa,\|}}{\tau_{el}^{\kappa,\|}} \approx 60 \tag{2.19}$$

   It indicates that the energy transport is dictated by the electrons and the ion energy fluxes just follow on a slower timescale. Such behaviour is typical for a stiff differential equation. In our case it requires an extremely precise determination of the larger electron energy flux to get a sufficiently good solution for the ion energy flux. Moreover one has to take into account a strong nonlinear and nonlocal coupling to the continuity equation and the momentum balance through the source terms.

2.4.2 Transport across field lines

The radial transport is the slowest process in the edge. Following the anomalous diffusion ansatz each physical quantity, particles, momentum and energy is crossing the field lines with a similar velocity of $(10 - 100)\frac{m}{s}$ typically.
The relaxation times for poloidal and radial transport differ by a factor of about 10. Assuming a nearly equal number of grid points in both directions this implies that the poloidal fluxes are ten times higher than the radial fluxes. We conclude that also with regard to the radial and poloidal momentum the model equations are stiff and need a careful treatment. It is evident that a small contribution from the poloidal velocity added to the radial velcotity may change the radial flux significantly and thereby the whole flux balance ($\rightarrow$ numerical diffusion)

2.4.3 The contribution of the source terms

The source terms can be divided into two parts: contributions from the plasma itself and contributions from other species.
The pressure gradient terms in the poloidal momentum equation and the energy exchange terms between electrons and ions belong to the first part. Because these sources

depend explicitly on the unknows, one has to solve the equations itertively until an equilibrium between the fluxes and the sources is reached.
The second contribution is more complex and difficult to handle. Here one has to consider the interaction of neutral particles and impurities with the plasma. From now on we will concentrate on the neutrals, since in our calculations only this species is selfconsistently included [1]. These neutral particles are generated at the target plates by surface-recombination of electrons and ions. From there they stream back and undergo complex interactions with the plasma (resulting in momentum sources, energy sources) until they are reionized (particle sources). The strength of the source terms is therefore

- for the various processes a function of the relevant reaction rate coefficients, strongly and nonlinearly depending on the electron or the ion temperature
- a function of the flux and its distribution over the target surface. Since the neutrals need a certain time to travel from the plate to the place of interaction, the coupling to the plasma state is thereby also non-local.

This discussion elucidates that the solution of our convection-conduction equations not only needs experience in "pure" numerics but mainly in "numerical physics" to know about the various aspects of the physical processes and choose an adequate numerical scheme which is capable to handle them.

[1] Until now the interactions with impurities are taken into account as a given quantity known either from measurements or from impurity transport codes

Chapter 3

Numerical methods for fluid equations

The most widely used techniques to solve convection-conduction equations in two or three dimensions are the finite volume method (FVM) and the finite element method (FEM). Finite volume methods are used since the beginning of computational fluid dynamics (CFD) and are more or less heuristically developed, whereas the finite element method in fluid mechanics has only a short history but it has a more sophisticated theoretical foundation.
Using the mathematical formalism of the FEM one can derive under certain assumptions the formulas of the FVM, show how the methods are related to each other and discuss the facilities of the different numerical schemes in general terms (Section 1).
In a second section the basic differences between the flow of gases and the flow of ionized particles are analysed. This leads to special requirements and stability criteria for numerical schemes, and it gives hints how these methods can be extended to handle the plasma fluid equations.
In Section 3 the geometrical discretization and the numerical procedure of the finite volume code B2 is explained and its adaption to our physical problem is discussed.
Section 4 contains an introduction to the solution procedures used for FEM-codes in other fields of CFD, whereas in section 5 the special numerical features of the SAFE-code will be adressed.
A concluding discussion of the strong and weak points of both procedures concerning the plasma flow in the edge of a TOKAMAK is given in Section 6.

3.1 General principles in CFD

To solve a system of differential equations numerically one has to discretize them (usually in time and space). Therefore the differentials are approximated by algebraic functions, which can be evaluated at certain points of time for a number of points in space. To achieve results which give a realistic approximation of the evolution in time and space one has to choose an appropriate spacing in the time and space coordinates. How this can be done is described in this section.

3.1.1 Discretization of convection-conduction equations

We consider a system of convection-conduction equations written in conservative form as

$$\frac{\partial}{\partial t}\vec{U} + \frac{\partial}{\partial x}\vec{F} + \frac{\partial}{\partial y}\vec{G} = \vec{S} \tag{3.1}$$

Integrating in time we get from the solution at time t_n a new solution at time t_{n+1} :

$$\vec{U}^{n+1} = \vec{U}^n - \int_n^{n+1} \left(\frac{\partial \vec{F}}{\partial x} + \frac{\partial \vec{G}}{\partial y} - \vec{S} \right) dt \tag{3.2}$$

Assuming a certain interpolation function within the time interval $\Delta t = t_{n+1} - t_n$ the integral is evaluated and can be characterized by a weighting factor α. Hence the new solution at t_{n+1} is:

$$\begin{aligned} \vec{U}^{n+1} &= \vec{U}^n - \Delta t \cdot \left\{ \alpha \cdot \left(\frac{\partial \vec{F}}{\partial x} + \frac{\partial \vec{G}}{\partial y} - \vec{S} \right)^{n+1} + (1-\alpha) \cdot \left(\frac{\partial \vec{F}}{\partial x} + \frac{\partial \vec{G}}{\partial y} - \vec{S} \right)^{n} \right\} \\ &\equiv \vec{U}^n - \Delta t \cdot \left\{ \frac{\partial \vec{F}}{\partial x} + \frac{\partial \vec{G}}{\partial y} - \vec{S} \right\}^{\alpha} \end{aligned} \tag{3.3}$$

For the discretization in space the computational domain with the area/volume Ω is subdivided into a number of **N cells** (area/volume Ω_i; $i = 1, ...N$).
In each cell the unknowns $\vec{U}$ are described by the values at the **K nodes** of the cell $\vec{U}_j^i$ $(j = 1, ...K)$ and by the **interpolation functions** N_j^i, which vanish outside cell i.
$\vec{U}$ is hence approximated by:

$$\vec{U} = \sum_{i=1}^{N} \sum_{j=1}^{K} N_j^i \cdot \vec{U}_j^i \tag{3.4}$$

To take into account the different size of the cells and to guarantee e.g. flux conservation equation 3.3 is integrated over the considered region, which can be done by summing up the integrals of all cells.
The multiplication of the kernel of each cell integral with a set of additional **orthogonal weighting functions** W_k^i $(k = 1, ...K)$ seems to be artificial but can be justified in the following way:

- The multiplication with a set of orthogonal functions will not change the solution itself.
- By choosing special weighting functions (depending on the solution or on the geometrical configuration) the numerical error within one cell and thereby over the whole domain can be reduced efficiently.

- Flux conservation can be maintained when the integral of the weighting functions over one cell is equal to 1.

For each weighting function W_k^i $(k = 1, ...K)$ equation 3.3 can now be written down discretized in time and space:

$$\sum_{i=1}^{N}\sum_{j=1}^{K} \left[(\vec{U}_j^i)^{n+1} \int_{\Omega_i} W_k^i N_j^i d\Omega_i\right] = \tag{3.5}$$
$$\sum_{i=1}^{N}\sum_{j=1}^{K} \left[\left\{(\vec{U}_j^i)^n + \Delta t(\vec{S}_j^i)^\alpha\right\} \int_{\Omega_i} W_k^i N_j^i d\Omega_i \right.$$
$$\left. - \Delta t \left\{(\vec{F}_j^i)^\alpha \int_{\Omega_i} W_k^i \frac{\partial N_j^i}{\partial x} d\Omega_i + (\vec{G}_j^i)^\alpha \int_{\Omega_i} W_k^i \frac{\partial N_j^i}{\partial y} d\Omega_i \right\}\right]$$

Remarks:

- The notation W_k^i for the weighting functions and N_j^i for the interpolation functions indicates that they are only defined in the cell i. For all other cells these functions are identically zero.

- The integrals in equation 3.5 are integrals over one cell and give contributions to each node of this cell. Summing up the integrals a certain node only gets contributions from the cells it belongs to.

After the discretized equations has been set up the solution procedure consists of the following steps:

1. Define a time marching scheme (Determination of the factor α).

2. Define the shape and the size of the cells.

3. Define the character of the weighting functions and the interpolation functions.

4. Determine the relation between the convective fluxes, the conductive transport and the source terms within one equation and analyse how strong they are related to the unknowns.

5. Take into account the dependencies between the different equations.

These steps are not in chronological order but strongly depend each on each other. So it's not the aim to make an optimal choice for one point but to find a numerical method where all requirements are at least marginally fulfilled.
In the next subsections each of these steps is described in more detail concentrating particularly on the relations between them.

3.1.2 Time marching schemes

Different time marching schemes are related to the choice of the relaxation factor α. This factor determines to which fraction of the fluxes and sources at time t_n and time t_{n+1} contribute to the new solution $\vec{U}^{n+1}$.
For $\alpha = 0$ the time evolution scheme is called "explicit" whereas for $\alpha > 0$ the scheme is called "implicit". These two methods require a totally different numerical treatment:

- $\alpha = 0$: **"explicit" method**
  To determine the new solution one only needs information from the last timestep, i.e. the right and the left side of equation 3.5 are decoupled. This method has the advantage that only the actual information on variables, fluxes and sources has to be stored. The disadvantage is that only this information is available and the changes within the timestep are not taken into account which leads to a restriction of the size of $\Delta t = t_{n+1} - t_n$.

- $\alpha > 0$: **"implicit" method**
  The new solution depends on the information from both times t_n and t_{n+1}. Thereby the left and the right side of equation 3.5 are coupled and assumptions on the change of fluxes (transport coefficient) and sources within the time interval have to be made. These changes can be calculated analytically or numerically. In any case it will increase the computing time per timestep, not only because of the additional operations but also because of the higher storage volume needed. This disadvantage may be overcompensated by the larger timestep (in relation to the explicit method) one can use. [1]

Even when no time evolution but only a stationary solution is considered a relaxation scheme has to be applied. This is mainly caused by the fluxes and source terms which depend in most cases strongly on the solution itself. Hence an iterative treatment of the equations is necessary to get a consistent solution.

Remark: For the iterative solution of the stationary equations also a timestep has to be introduced and must be adapted to the typical transport velocities and the cell size. ($\Rightarrow$ relation between timestep and cell-size)
The discussion on the discretization in time applies to both finite volume methods (FVM) and finite element methods (FEM). Differences between the two schemes arise with regard to the discretization in space.

3.1.3 Discretization in space and integration formalism

Since the considered differential equations are two-dimensional in space we will restrict our discussion to discretized planar geometries and the integration over two-dimensional cells. Moreover we will not discuss grid generation (subdivision of a computational domain into cells) but direct our attention to different cell-types (triangles, quadrilaterals) and interpolation/weighting functions commonly used in FVM

[1] There are also schemes which require information from more than two times. For these schemes the storage problems are even larger but the time evolution is more stable for a given timestep

and FEM respectively.

Two-dimensional grids for the FVM

Mainly because of the heuristic development of the FVM one is forced to use simple quadrilaterals with four nodes as cell type. Generally these cells are aligned to the coordinate directions and build up a structured mesh which has everywhere a fixed number of cells in each direction. The great advantage of the structured mesh is the regular numbering of cells and nodes, which creates a structured equation system and makes it easy to find the next neighbours. But using such meshes two serious problems are unavoidable:

- Complex geometrical structures can only be described if
  1. a conformal mapping procedure can be used to transform the given domain into a rectangle. In some cases it is possible but a numerically demanding transformation must be applied, in most of the cases it is quite impossible.
  2. if a large rectangle is overlaid over the whole domain and the cells outside of the computational domain are "blocked off" in the calculation. This process seems to be very promising but is numerically difficult. One has to impose boundary conditions for cells in the interior of the mesh. Secondly it must be guaranteed that the cells outside of the considered geometry - which still exist in the calculation - will not change the solution.
- In general a refinement of the grid to resolve strong gradients in a little area requires a denser mesh all over the domain. Local grid adaption is only possible when "multigrid" methods are used. "Multigrid" means that in the interesting region additional new nodes are created between old nodes and thereby a new regular grid is created in this area which has it's own boundary at the transition from the fine to the coarse grid. For the nodes at this boundary belonging to the new but not to the old mesh ("hanging" nodes) one has to employ numerical procedures to interpolate from the coarse mesh to the fine one and vice versa. Such methods are not only complex from the numerical point of view but also need a lot of experience to decide
  1. how far the finer grid has to be extended
  2. how the relaxation for the different grids has to be organized.

Two-dimensional grids for the FEM

The most widely used element type for FEM are triangles. The meshes are unstructured and no orientation to special coordinates is necessary. Thereby one has no problems to create meshes for complex geometries.
The numbering of the cells and nodes is not regular and one has to use a local cell numbering, a global node numbering and a procedure to get from one to the other. Only through this indirect addressing it is possible to find next neighbours. Until about ten

years ago this numerical procedure makes information exchange between the cells and the global mesh extremely slow and vectorization operation impossible. Today these computer problems are solved and the indirect adressing has no drawback.
Moreover the triangular cell-type along with the indirect adressing procedure are necessary to apply solution adaptive local mesh refinement without creating hanging nodes. Such grid size adaption in regions with strong gradients permits a reduction of grid points by approximately a factor of $2-3$ with respect to a completely refined regular mesh [1].

Relation between cell-type and interpolation functions

For each of the K nodes in cell i a specific interpolation function is introduced so that the variables $\vec{U}$ at each point (x,y) within the cell can be approximated:

$$\vec{U}^i(x,y) = \sum_{j=1}^{K} N_j^i(x,y) \cdot \vec{U}_j^i \tag{3.6}$$

To reproduce the node values exactly the interpolation functions must be equal 1 at the node they belong to and zero at all other nodes:

$$N_j^i(x_j,y_j) = 1 \qquad N_j^i(x_k,y_k) = 0 \quad (k \neq j) \tag{3.7}$$

These equations determine K free parameters $(a_j^i, b_j^i, c_j^i, ...)$ for each $N_j^i(x,y)$, independent of the functional dependencies $f(x), g(y)$ (linear, quadratic, exponential,...).
Especially for triangles and quadrilaterals the interpolation functions have the form:

- interpolation functions for triangles:
  $N_j(x,y) = a_j + b_j \cdot f(x) + c_j \cdot g(y) \qquad (j = 1,2,3)$
- interpolation functions for quadrilaterals:
  $N_j(x,y) = a_j + b_j \cdot f(x) + c_j \cdot g(y) + d_j \cdot f(x)g(y) \qquad (j = 1,2,3,4)$

Weighting functions

The appliction of weighting functions is only optional and a special feature of the FEM. In the FVM all integrals have the same weight and are multiplied with a factor 1/K (K: Number of nodes per element), hence the weighting functions are spatially constant.
The common way to choose them in FEM is the galerkin approach: For weighting and interpolating the same set of functions is used.

Relation between the integration schemes of FVM and FEM

In general it's difficult to compare the integration formalism of FVM and FEM because of the different cell-types [2], the different weighting functions and the various forms of interpolation functions which can be used. Nevertheless for a simple case the schemes can be related to each other. This comparison may stimulate and hopefully

[2] Although in the FEM quadrilateral can be used, we will here concentrate on triangles.

will simplify further discussions on the numerical accuracy of both methods.
It can be shown (see Appendix A) that for a simple convection equation the FEM with linear interpolation functions delivers the same flux balance in a certain point P as a 9-point-scheme in FVM (all nodes of the adjacent cells influence the flux balance in P). For the case of rectangular cells each direction (x,y) can be treated quasi one-dimensional and all fluxes are divided up in a part parallel to the x-direction and a second part parallel to the y-direction. Only in such grids the simple and widely used 5-point-scheme (2 points are connected to a point P in x-direction and y-direction respectively) is applicable.

Numerical Diffusion

Numerical diffusion is a discretization error and occurs when the flow is oblique to the grid lines und when there is a nonzero gradient of the dependent variable in the direction normal to the flow. Each numerical scheme shows such errors but in different methods they are more or less suppressed.
Consider a flux flowing in diagonal direction through a rectangular grid and no transport orthogonal to the flow direction should be possible. If the 5-point-scheme is used the flux in each cell is decomposed in a part along the x-direction and a part along the y-direction and from cell to cell only information along x and y is passed on. This leads to a fan-shaped flux distribution only introduced through the numerical solution scheme.
If for the same situation a 9-point-scheme or a finite element solver is used point P gets information from all surrounding points including the one diagonal opposite to P (in flow direction). This will reduce the error and guide the flux in the right direction but a certain numerical diffusion will remain [6].
It can be stated that if the flow field is not aligned to the grid directions the numerical diffusion error for the FEM and the 9-point-scheme in FVM is much lower than for the 5-point-scheme even in a rectangular grid. But -as will be shown later- in a strong anisotropic case the remaining numerical diffusion will play a major role.

3.1.4 Relation between the discretization in time and space

As was stated in section (2.4.1.) the typical transport processes for the plasma-fluid equations are convection, sound wave propagation and a certain amount of conduction [3]. Thereby one has for the ions a maximal energy transport velocity of

$$V^{ion} = (2 + F_i) \cdot c_s \qquad (F_i : Flux\ limit\ factor\ ;\ c_s = \sqrt{\tfrac{T_i+T_e}{m_i}} : sound\ velocity)$$

For the electrons the transport velocity including flux limited conduction is

$$V^{el} = (1 + F_e) \cdot v_{th} \qquad (F_e : Flux\ limit\ factor\ ;\ v_{th} : electron\ thermal\ velocity)$$

Multiplying these velocities with a chosen timestep Δt one gets typical transport lengths parallel to the magnetic field which can be projected into the poloidal plane

[3] By introducing a flux limit factor F_i the conductive transport is limited to $Q_{cond} \leq F_i \cdot Q_{sound}$

giving:

$$l_{pol}^{ion} = b_\theta V^{ion} \cdot \Delta t \approx 10^4 \tfrac{m}{s} \cdot \Delta t$$

$$l_{pol}^{el} = b_\theta V^{el} \cdot \Delta t \approx 3 \cdot 10^5 \tfrac{m}{s} \cdot \Delta t$$

Considering now a certain node in the mesh all points in poloidal direction within l_{pol}^{ion} and l_{pol}^{el} will contribute to the ion energy and the electron energy respectively in this node. Therefore the information from all these nodes has to be included in the solution procedure to prevent physically induced numerical instabilities.

Explicit method:
One way to guarantee stability is to use such a small timestep that the grid spacing Δx_{grid} is larger than the transport length:
$\Delta x_{grid} \geq l_{pol}^{ion} \approx 10^4 \tfrac{m}{s} \cdot \Delta t$
$\Delta x_{grid} \geq l_{pol}^{el} \approx 3 \cdot 10^5 \tfrac{m}{s} \cdot \Delta t$
This implies that only next neighbour nodes can exchange information which is easy to compute. But as the timestep is so small a lot of iterations are needed to get a stationary solution. For example near the target the poloidal grid spacing should be in the range of $\sim 1cm$ which leads to timesteps for the ions of the order $\Delta t_{ion} \sim 10^{-6}s$ and $\Delta t_{el} \sim 10^{-8}s$ for the electrons. As the time for the whole system to relax into an equilibrium is of the order of $10^{-3}s$ one needs about 1000 iterations for the ions but nearly 100.000 iterations for the electrons. These relations are another typical feature of a system of stiff differential equations.

Implicit method:
When a larger timestep is used many nodes are interacting with each other and therefore a large equation system has to be solved. This needs a lot of computing time, but with respect to the explicit method the number of iterations is smaller and non-local effects, e.g. from source terms are taken into account.
Even for the implicit method the timestep is restricted. One has to guarantee that the transport coefficients and the source terms are not changing too much from t_n to t_{n+1}. Because of the strong nonlinearities one is forced to use a timestep which at the most is about ten times larger than the explicit one.

An extension of the implicit timestep is possible if the changes of the transport coefficients and source terms are taken into account. This can be achieved by decomposing the nonlinear terms into a constant part and a part linearly depending on the unknowns, e.g. for the heat conduction coefficient one gets:

$$\kappa(T) = \kappa_0 + (\frac{\partial \kappa}{\partial T})_0 \cdot (T - T_0) \tag{3.8}$$

Terms of higher order are neglected. The same procedure can be applied to expand the source terms.

3.1.5 Relation between convection, conduction and sources

The solution of a convection-conduction equation including sources depends strongly on the character of the differential equation, which is related to the strength of the different terms. Consider such an equation in one dimension describing the plasma flow along field lines [4]:

$$\frac{\partial \Phi}{\partial t} + \rho u \cdot \frac{\partial \Phi}{\partial x} - D \cdot \frac{\partial^2 \Phi}{\partial x^2} = S \tag{3.9}$$

A stationary solution can be found by solving the characteristic polynomial:

$$\rho u \cdot \lambda - D \cdot \lambda^2 = S \tag{3.10}$$

Thereby we get the solution:

$$\Phi(x) = c_1 \cdot e^{\lambda_1 x} + c_2 \cdot e^{\lambda_2 x} \tag{3.11}$$

with the characteristic variables

$$\lambda_{1/2} = \frac{\rho u}{2D}\left(1 \pm \sqrt{1 - \frac{4D^2 S}{\rho^2 u^2}}\right) \tag{3.12}$$

For the limit of a diffusion dominated transport ($\lambda_{1/2} \ll 1 \quad \rightarrow \quad e^{\lambda x} \approx 1 + \lambda x$) the spatial variation of Φ is linear, a convection dominated transport leads to an exponential profile and including strong sources the solution changes to a combination of exponential and trigonometric functions.
In the plasma edge all these features are present:

- Diffusion dominates the transport in the symmetry plane
- Convection becomes more and more important along the field line up to the target
- Because of strong recycling the sources in front of the limiter are as important as convection.

The solution procedure should be capable to handle these cases by using different interpolation functions depending on the strength of fluxes and sources.

In addition to that a numerical difficulty arises in the calculation of velocity and pressure fields. It's mainly a problem of the first derivatives in the poloidal momentum equation which may produce oscillations, where from one to the next grid point pressure is transformed into velocity and vice versa ("grid sound waves"). This process is superimposed on the normal sulution and therefore will not be damped out. The common way to prevent such oscillations in FVM is the introduction of a staggerd grid (calculation of pressure and velocity on shifted grids). In FEM such oscillations are suppressed by using a higher order interpolation function for the velocity than for the pressure (Babuška-Brezzi-criterion).

[4] This is a good approximation for our problem since the radial fluxes can be treated as sources (section 2.4.1)

3.1.6 Coupling of the variables density, momentum and energy

Until now only one equation of convection-conduction type is considered; But in our case a system of equations describes the flow of particles, momentum and energy. Thus one has to take into account the coupling between these equations. Besides the effects caused by changes in the transport coefficients and source-terms discussed before an important coupling parameter is the pressure. Following the ideal gas law a species α has the pressure $p_\alpha = n_\alpha \cdot T_\alpha$ where n_α is the density of the gas and the temperature T_α represents the isotropic mean quadratic velocity $v_{th}^2 = \int(\vec{v})^2 f(\vec{v}) d\vec{v} = \gamma T_\alpha / m_\alpha$. So the pressure as a product of density and temperature is influenced by the particle fluxes and energy fluxes. However it's gradient acts as a source term in the momentum balance and thereby density, flow velocity and temperature are coupled. Depending on the strength of the interference one distinguishes two different situations:

- **The incompressible flow**
  If the flow velocity relative to the sound velocity or the thermal velocity is low the temperature remains nearly constant. This means that the continuity equation and the momentum balance are coupled, whereas the energy equation is separated from these. In such a case the pressure gradient is only related to changes in density and can be calculated using the ideal gas law and the actual value of the density. For the temperature it is sufficient to apply the value of the preceding iteration.

- **The compressible flow**
  If the flow velocity is of the order of the thermal velocity, changes in flow velocity will influence the temperature and vice versa. In this case the pressure gradient force depends on particle fluxes and energy fluxes. Variations in both values have to be considered to get a good approximation for a new momentum balance, e.g. by solving a separate convection-conduction equation for the pressure (pressure-correction-equation).

For both cases it may be helpful to introduce a linearization scheme (Newton-Raphson-method) to include the nonlinear dependencies not only within one equation but also between different equations. The major disadvantage of this method is that the solution algorithm becomes complex and time consuming and finally it's not clear whether a linear expansion is a reasonable approximation for the nonlinear terms and leads to a higher rate of convergence.

3.2 Special features of the plasma flow compared to the flow of neutral gas

Consider the flow of ionized particles outside the separatrix between the symmetry plane ($\vec{v} \approx 0$) and the target plates, where the ions should reach sound velocity ($\vec{v} = c_s$). This situation is comparable to the flow of neutral gas in a jet or a nozzle with the following typical boundary conditions: at the entrance the flow velocity

should be low, whereas near the outlet the particles switch to transsonic velocity. But the behaviour of both fluids inside the considered domain is quite different. It can be explained by analysing the characteristics (eigenvalues) of the time-dependent two-dimensional differential equations describing the systems (→ section 2.1).).

3.2.1 The flow of neutral gas

Since diffusive fluxes of momentum and energy are small compared to convective fluxes and since external forces are not taken into account the characteristics of the model equations are nearly the same as for a purely convective flow. In this case the transport laws are symmetric in each direction and the components of the velocity in each spatial direction $(\vec{u}, \vec{v})$ can be added up to give an effective flow velocity $(\vec{w} = \vec{u} + \vec{v})$, which is a twofold eigenvalue (two-dimensional geometry) [5]. Because of this isotropic behaviour the transport of a physical quantity Φ (density, momentum, energy) is described by a flux $\vec{\Gamma_\Phi} = \vec{w} \cdot \Phi$ along the direction of $\vec{w}$. A numerical procedure using such effective fluxes can be set up to calculate a flux balance between adjacent grid points. Especially for the FEM or for a 9-point-FVM the grid lines may not necessarily be parallel to the flow direction because numerical diffusion errors are strongly reduced.

3.2.2 The flow of plasma

The ionized particles in a plasma behave totally different because of their electric charges. The cross-section for collisions is larger than in a neutral gas and has a long range. On a macroscopic length scale these interactions can be described through diffusive fluxes, appearing either between electrons and ions or within the same species [1] .
The coupling of different components of the plasma is described through exchange terms of momentum and energy in each fluid equation. These source terms are strongly depending on electron temperature and density. Such nonlinearities require an iterative solution procedure.
The strong interactions between particles of the same species cause a remarkable perturbation of their free streaming flow. For typical temperatures and densities in the plasma edge ($T \approx 20eV$; $n \approx 10^{18}m^{-3}$) these diffusion-like effects are as important as the convective fluxes, so that the Reynolds-number and the Peclet-number are in the order of 1. Using these scale-invariant numbers the plasma flow is comparable to the flow of glue.
Remark: Glue and plasma are not only comparable because of their similar flow properties but also with respect to their microscopic structure: Glue is composed of a negatively charged solvent and solved particles with a positive charge. Moreover the mass ratio of the solvent (alcohol) to the solved polymer molecules is about 1:100. So one may identify the solvent with the electrons and the polymer with the ions.

[5] One get's the remaining two eigenvalues by adding and subtracting the sound velocity

Another decisive difference to the flow of neutral particles is the influence of external fields on the particle motion in a plasma. Besides the response on electric fields, discussed in detail in the work of M. Baelmans [2], the various plasma species are flowing strongly aligned to magnetic field lines ($\| \vec{B}$). Even perturbations of this field structure, leading to experimentally observed higher fluxes $\perp \vec{B}$, do not destroy the nearly one-dimensional behaviour. Such strong anisotropic flows are a great challenge for numerical methods. They have to guarantee that the "diffusion" errors produced by the discrete approximation of the fluid equations are much lower than the physically realistic fluxes.

Compared to the flow of neutral gas a qualitativly new, non-local and non-linear effect occurs because of the interaction of the ions and electrons with neutralized plasma particles, generated at the walls. Several difficulties arise from this situation:

- The motion of neutral particles is not influenced by the magnetic field and thereby different coordinate systems are necessary to describe the flow pattern of both species physically realistic.

- The flux of neutralized particles from a wall back into the plasma is proportional to the flow velocity of the ions, which depends on the plasma temperature in front of the wall. But this temperature is strongly influenced by the interactions of the neutral particles with electrons and ions. Because the energy exchange rate is a highly nonlinear function of the plasma temperature a consistent solution is only achieved after a large number of iterations.

- The flux of the neutralized particles is proportional to the density of the ions near the target. Because of the reionization of neutrals the plasma density is increased and a feedback process is initialized. Since the number of the neutrals, reionized at a certain distance from the targets (ion source), depends on the ion flux onto the plates one has a non-local coupling of sources and fluxes over a distance of several cells.

However the separation of these effects is artificial and connections between them exist through the balances of particles, momentum and energy. In particular in the case of high reionization rates such nonlinear interdepencies play a major role. They reduce the convergence rate and thereby render the solution procedure.

3.3 The finite volume code EB2

In this section the special features of the FV-code EB2 are introduced and it's adaption to the different requirements of the plasma-fluid equations are discussed.

3.3.1 The spatial discretization

Starting from a magnetic equilibrium in a TOKAMAK with given flux surface structure a conformal mapping procedure is used to transform the geometrical configuration in real space into a rectangle in an imaginary space. The domain is then subdivided into orthogonal quadrilaterals aligned to the magnetic field lines, so that two sides are parallel to $\vec{B}$ and the other sides are prependicular to $\vec{B}$.

The transformation of a limiter configuration or a divertor geometry into a rectangle implies that field lines, which are closed in the real space have to be "cutted" in the imaginary space. The generation of these "cuts" is topologically necessary and thereby it's unavoidable that next neighour cells in real space are separated in the imaginary space and additional boundary cells are created. These cells are either treated as "isolated", "explicitly" or "implicitly" coupled.

- **Case 1: Isolated cut cells**
  The cut cells are totally separated and next neighbour cells in real space don't have any contact in imaginary space. The solution gained by inversion of a structured and symmetric matrix shows discontinuities at the cuts and therefore is only a crude apporximation. Moreover if the cuts are placed in regions where strong gradients may occur, e.g. near target plates, the solution is not meaningful at all.

- **Case 2: Explicitly coupled cut cells**
  The simple solution algorithm of case 1 is applied iteratively. After each iteration the values of the variables and fluxes at the artificial boundaries are corrected using an interpolation procedure between these cut cells, which are adjacent to each other in real space. After a certain number of iterations a "consistent" solution can be achieved. It should be remarked that the term "consistent" in this case is not strictly defined since in the cut cells even the interpolation acts as a special type of boundary condition; for the variables and also for the fluxes either constant values or constant derivatives can be required.

- **Case 3: Implicitly coupled cut cells**
  Additional equations (Lagrangian-conditions) are formulated, which reconnect the cutted cells. These equations are added to the ordinary equation system. Thereby the structure and symmetry of the old system is broken and more complex solution methods must be applied; but within each iteration step the fluxes and variables at the artificial boundaries are selfconsistently determined.

All these cases are in use. Case 1 is mainly applied to get a first approximation - a seed plasma - from which the exact solution can be derived using case 2 or case 3. There is no first choice whether to use explicit or implicit coupling. The explicit method is easy

to compute because of the simple structure of the equation system [6] but needs a lot of iterations to achieve a consistent solution. For the case of implicit coupling one has to solve an equation system with band structure. The solution procedure for such a system indeed requires more computer time per iteration but fewer steps are necessary.

Moreover the alignment of the cells to the magnetic field, the mapping procedure and the regular mesh numering makes it difficult to take into account additional boundary structures intersecting the field lines. This problem can only be solved when regions covered by target tiles or baffles are "blocked off". A recently developed method proceeds as follows:

- The commonly used mapping procedure transforms the magnetic field structure into a rectangle and defines orthogonal, regular numbered grid cells.
- The intersection points of the additional boundary structures with the grid cells are determined.
- The corners of the concerned cells are shifted to the intersection points and the dimensions of the cells are recalculated.
- The modified mesh must retain the regular structure and should only violate the orthogonality in the new created boundary cells.
- Boundary conditions are formulated at the new border. Inside the "blocked off" region the variables and fluxes are choosen to fulfill these conditions.

The applicability of the scheme has been demonstrated and it is used in this work to describe the geometry of a pumplimiter. But in general it needs a lot of experience to decide in which way cells should be distorted to avoid errors in the numerical scheme and to reduce numerical diffusion errors. So it is not a standard tool even for our flow problems showing strong anisotropy in the flow field.

3.3.2 The solution procedure

The time marching sheme

The EB2 code solves for each plasma-variable Φ such as density, poloidal velocity, ion temperature and electron temperature a stationary fluid equation iteratively. The method is comparable to a fully implicit time evolution scheme using an underrelaxation factor instead of an exact time-integration-method.

Remark:
Each convection-conduction-equation is solved in a linearized form assuming constant transport properties, characterized by the diffusion coefficient, the convective fluxes and the source terms. These quantities are taken from the last iteration and their dependence on the new results is neglected. So far the method is not "fully" implicit.

[6] This is based upon the regular numbering of the mesh

Solution in the spatial coordinates

Because the grid cells are orientated with respect to the characteristic transport directions of the plasma flow – parallel and perpendicular to the magnetic field – the numerical diffusion is strongly suppressed and a simple 5-point-scheme can be used to solve the discretized fluid equations. For such an orthogonal grid even a 9-point-solver will not further reduce this discretization error.
Integrating the convection-conduction equation in each cell and for each variable (density, poloidal and radial ion velocity, ion temperature and electron temperature) various interpolation functions can be choosen. For most calculations the hybrid scheme or the power law scheme are applied. Both methods are approximating the solution of the one-dimensional convection-conduction equation with constant coefficients ($\rightarrow$ 2.17).
For simplification of the numerical procedure the hybrid scheme assumes a piecewise linear dependence on the Peclet-number, which gives a reasonable accuracy to the exact exponential behaviour. The power law scheme approximates the exact solution within 1% but is not as easy to compute as the hybrid scheme [4].

Treatment of nonlinear terms and source terms

Within the equation for each variable the components of the flow velocity and the transport coefficients are assumed to be constant. They are determined using the values of the variables of the former iteration. In contrast to another FVM [7] their changes are not taken into account. Thereby the underrelaxation factor must be smaller compared to [7] and one has no direct (implicit) coupling between the density, the momentum and the energy. Instead of this the different equations are explicitly coupled using a special relaxation procedure. Starting from a given flow field and constant transport coefficients a sequence of equations is passed through:

1. The parallel momentum equation is solved to correct the poloidal velocity.
2. The radial momentum equation is calculated according to the density profile.
3. A pressure correction equation is solved to take into account the propagation of sound waves, i.e. the effects of compression on both the flow velocity and the density.
4. Using the new values of the density and the fluxes the ion temperature and the electron temperature are relaxed separately.
5. An equation for the total energy is solved to include the temperature changes because of internal energy exchange between ions and electrons.
6. Corrected values for T_e and T_i are obtained from the two steps before and since the transport coefficients are strongly depending on ion and electron temperature the flow field must be calculated once again. (step 3).

This procedure is repeated until convergence is achieved.

The external sources of particles, momentum and energy, arising from interactions with neutrals or impurities, are considered as additional fluxes after multiplication with a characteristic timestep. This timestep is restricted because of the strong dependence of the sources on ion and electron temperature and because of the choosen solution algorithm.
Concerning the nonlinearities in the temperatures the timestep can be extended using a linear expansion like the one in equation 3.8.
The second restriction is more severe. Both the interpolation functions and the sequential treatment of the fluid equations are derived for convection-conduction dominated transport. Therefore the timestep has to be reduced until the contributions from the sources are small compared to the convective and conductive fluxes. Whereas far from the target plates this condition poses no problem, it plays a major role in regions with strong sources. There the character of the solution is changing as it has been shown before (section 3.1.5.).
Using different interpolation functions, not only depending on the Peclet-number but also on the strength of the source terms, will help to overcome this disadvantage. Moreover strong variations of the source terms within one cell can be taken into account. This leads to a better approximation of the cell integrated source strength compared to the linear interpolation used up to now.

3.4 Finite element methods in CFD

In this section the solution of fluid equations using the FEM is illustrated. Starting point of our considerations is the present status of the FEM in "conventional fluid" dynamics. Different numerical approaches are presented and their applicability to certain flow regimes is discussed.
Thirty years ago the first FEM-codes have been developed to describe and solve problems of diffusion-type (second derivatives). Their great advantage compared with FVM-codes is related to the generalized integration formalism, which allows for a non-orthogonal, unstructured spatial discretization.
First attempts to include convection (first derivatives) in FEM were made $\sim$ 1975. Nowadays it has become a common tool for the numerical calculation of air flows, which are convection-dominated. Because of the great geometrical flexibility of the method most of the work is concentrating on questions concerning mesh generation and solution adaptive mesh refinement in two and three dimensions. Only a slight progress has been achieved concerning the numerical solution of the discretized differential equations, mainly because the character of many modelled processes is nearly the same; in most cases the calculations simulate the flow of a single species at lower temperature ($T \leq 1000\,K$) and with high Reynolds-number in a cavity with complex boundary structures.
For such situations two typical (time-dependent) solution schemes are used:

- an **explicit praedictor-corrector method** [8] and
- an **implicit Newton-Raphson method** [9].

3.4.1 Explicit praedictor-corrector method

This method is simple both from the mathematical and the computational point of view. Linear interpolation and weighting functions are used for all variables so that the volume and surface integrals can be calculated analytically. Thereby the differential equation splits up into simple algebraic equations, one for each node in each element, describing a discrete time evolution of the considered variables. Starting point of the calculation is the solution at a time t_n. After a timestep Δt a new solution at a certain node is found by summing up the contributions from the sorrounding elements at time t_n, multiplying this effective flux by Δt and adding it to the old value. For time-independent boundary conditions a stationary solution is found, when the simulated time is much larger than the characteristic timescale for the slowest transport process (macroscopic relaxation time) .
As indicated above (section 3.1.5.) the choice of linear functions for **all** variables in general leads to numerical instabilities, when the fluxes are direct proportional to the external forces [7]. The formation of such instabilities can be suppressed when a two-step-scheme is applied. In a praedictor step new values for the unknowns are calculated considering only convective transport phenomena. Then in the corrector step – using the flow velocities from the first step – all transport processes are taken into accoount. This implies that the convective fluxes are determined two times, which is equivalent to a quadratic interpolation. The other variables – diffusive fluxes and source terms – are approximated only by linear functions and so the Babuška-Brezzi-criterium (→ 3.1.5) is fulfilled.
The simplicity of the explicit time marching scheme is due to the restriction of the timestep so that only neighbouring elements can influence the solution at a certain node. No global flux balance has to be fulfilled and thus complicated matrix operations are avoided. On the other hand this "local" treatment may require a lot of iterations to find a stationary solution. It depends on the ratio of the macroscopic relaxation time and the microscopic timestep how many iterations are necessary. The macroscopic timescale is defined through the typical length of the calculation domain and the average flow velocity:
$\tau_{mac} = \frac{L}{\overline{v}}$.
Microscopic timesteps can be calculated for each node i of the grid as the quotient of the typical cell size and the maximal transport velocity:
$\tau_{mic,i} = (\frac{\Delta l}{v_{max}})_i$.
The smallest timestep must be chosen to achieve numerical stability for all nodes:
$\tau_{mic} = min\{\tau_{mic,i}\}$.
Since the average flow velocity is much lower than the maximal transport velocity the number of iterations can be estimated:
$N_{it} \geq \frac{\tau_{mac}}{\tau_{mic}} \gg \frac{L}{\Delta l} \geq N_{cell}$
(N_{cell}: number of cells along the flow direction)
For "conventional" gas flows at room temperature the maximal transport velocity is the velocity of sound, mainly determined by the temperature of the gas.
The effects of viscosity and heat conduction play only a minor role ($Re \approx Pe \approx 10^7$) and do not significantly change the convective fluxes. Even the strong nonlinearities

[7] A stable algorithm requires a linearity between the fluxes and gradients of the driving forces

in the transport coefficients are negligible and so the assumption of constant values for each timestep is an excellent approximation.
The nonlinear coupling between the flow of particles, momentum and energy through pressure changes is taken into account applying an equation of state after each praedictor step. This approximation is numerically stable as the pressure changes are only caused by convective transport and therefore the maximal propagation velocity is the sound velocity.
Interaction with other fluids or external sources of particles, momentum or energy are not included. Only suggestions have been made to take into account physical or chemical reactions. [10]

3.4.2 Implicit Newton-Raphson method

Implicit solution algorithms using the Newton-Raphson method are mainly developed for convective flows at high Reynolds-numbers without sources inside the calculation domain. In such cases the weak nonlinearities within one equation and also between different equations can be expanded to first order in the unknowns (Jacobian-matrix). The dependencies of the different terms on the variables can be evaluated analytically. Changes in pressure are expressed and explicitly calculated as changes in density and temperature. The derived linearized equations are in nearly all algorithms integrated on a triangular grid following the Galerkin-approach with linear interpolation functions. But even under these simplifying assumptions a criterium for the convergence of the method is difficult to determine.
The application of the scheme to complexer flows with large convective fluxes in one region, strong diffusive fluxes in another part of the calculation domain and spatially localized nonlinear source terms using a analytically determined Jacobian-matrix and linear interpolation is difficult and may be errorprone. First attempts have been made to introduce numerically calculated Jacobians – a common tool in FVM – and higher order interpolation functions.
Numerically calculated Jacobians take into account the correlations between one unknown and all others and in this way strong nonlinear dependencies can be included. **Higher order interpolation functions** are often applied together with adaptive mesh refinement procedures (h-p-methods). The purpose of both methods is to resolve large gradients either by a better approximation of the solution in each cell or by a finer grid structure. Although the results obtained for one-dimensional test-cases are of great promise, schemes for general transport properties on at least two-dimensional grids are not yet available.

3.5 The finite element code SAFE

In this section the numerical features of the SAFE-code are introduced. Especially the spatial discretization and the solution procedure of the SAFE-code are described showing how the code – originally developed for compressible air flow at room temperature – is adapted to the dynamics of plasma flow.

3.5.1 The spatial discretization

At first the plasma edge region is decomposed into rectangles. Each rectangle is then divided into two triangles. For these cells and for the grid points the direction and the strength of the magnetic field is evaluated by interpolation of the results of an external equilibrium calculation. Through a local coordinate transformation (rotation of grid cells) the interpolation functions and the weighting functions, formulated in general coordinates, are mapped into functions along and perpendicular to the magnetic field.

Remark: Instead of the transformation of the geometry it may also be possible to transform the fluid equations from the characteristic directions into general coordinates. But in this approach the structure of the equations will be destroyed and the formulation of vector relations and higher order derivatives will generate very complex expressions. Moreover the interpretation of the results is much more difficult.

Such a formulation in local coordinates is only possible using the FEM. Through the scalar multiplication of the differential equations with orthogonal weighting functions the overall flux balance can be expressed as a sum of balances over the grid cells [8]. Strongly related to this elementwise treatment is the unstructured discretization of the calculation domain without regular numbering of nodes and elements. An information exchange between the cells and the global geometry is realized using a global node numbering, a local numbering within each element and an indirect adressing procedure to switch from one to the other. Thereby not simply connected regions with complex boundaries are easily discretized and – even in the case of triangles – a local grid refinement can be applied.

Although the transformation into magnetic fields coordinates is practicable without regard to the shape of the elements, the effects of numerical errors must be taken into account.
Discretization errors because of the strongly different flow velocities in radial and poloidal direction are reduced when the elements are stretched in poloidal direction, so that the fluxes over each side of an element are of the same order of magnitude. A nearly equal resolution in both coordinates can be achieved in a mesh with approximately N grid points in radial direction and $2 \cdot N$ grid points in poloidal direction ($N \approx 15 - 30$).
Numerical errors because of the specific approximation of derivatives in the differential equations (numerical diffusion) are still remaining. They can be strongly suppressed when the elements are aligned to the characteristic directions of transport. In our case one side of each triangle is therefore oriented parallel to a magnetic flux surface and a second one perpendicular it. But in contrast to the finite-volume discretization, where by definition the orthogonal cells are exactly adapted to the field, the finite-element triangles are only approximately aligned. Although the deviation angle is less than 5° "numerical diffusion" may pose a serious problem because of the strong anisotropy in the flow velocities [6].

[8] Remember that in the FVM no weighting functions are used !

3.5.2 The solution procedure

The time-dependent explicit Taylor-Galerkin approach explained in section 3.4.1 is used to solve the discretized ion fluid equations. Originally developed for convection-dominated flows [8] the scheme is extended to take into account source terms of particles, momentum and energy. Moreover an additional energy equation for a second species (electrons) is considered. Since the integration formalism of the FEM is explained in detail in a preceding work [1], the discussion will concentrate on the specific numerical treatment of the plasma equations.

Determination of the timestep

For the simulation of a neutral gas flow at room temperature ($Re \approx 10^7$) the size of the timestep is characterized by the sum of convective flow velocity w and sound velocity c_s and the length l_w of the smallest grid cell in flow direction:

$$\Delta t \leq \tau_{conv} = \frac{l_w}{w+c_s}$$

Timestep for the ion species: For the ion species in the plasma fluid not only convection and pressure propagation but also diffusive transport and creation or annihilation of particles, momentum and energy must be considered. Including all these effects the size of the timestep decreases compared with the one in the pure convective case. It is derived from the equations (2.1 - 2.6), which can be written in a generalized form describing the variations of parallel velocity ($U = v_{||}$) as well as the changes in ion temperature ($U = T_i$):

$$\frac{\partial U}{\partial t} + (v_{||} + c_s) \cdot \frac{\partial U}{\partial x_{||}} - \frac{\partial}{\partial x_\perp}\left(\frac{D}{n}\frac{\partial n}{\partial x_\perp} \cdot U\right) = \frac{\partial}{\partial x_{||}}\left(\chi_{||}\frac{\partial U}{\partial x_{||}}\right) + \frac{\partial}{\partial x_\perp}\left(\chi_\perp \frac{\partial U}{\partial x_\perp}\right) + S_U \quad (3.13)$$

Assuming constant transport coefficients an upper limit for the timestep can be evaluated from equation (3.13):

$$\Delta t_{ion} \leq \frac{\tau_{conv}^2}{2}[\tau_{D,\perp}^{-1} + \tau_{\chi,||}^{-1} + \tau_{\chi,\perp}^{-1} + + \tau_S^{-1}]\left\{-1 + \sqrt{1 + \frac{4}{\tau_{conv}^2(\tau_{D,\perp}^{-1} + \tau_{\chi,||}^{-1} + \tau_{\chi,\perp}^{-1} + \tau_S^{-1})^2}}\right\} \quad (3.14)$$

τ_{conv}, $\tau_{D,\perp}$ $\tau_{\chi,||}$, $\tau_{\chi,\perp}$ and τ_S are typical transport times of parallel velocity or temperature in a certain cell of the length $l_{||}$ along the magnetic field and of the width $l_\perp$ perpendicular to the field lines:

$$\tau_{conv} = \frac{l_{||}}{v_{||}+c_s} \quad ; \quad \tau_{D,\perp} = \frac{l_\perp^2}{2D_\perp}$$
$$\tau_{\chi,||} = \frac{l_{||}^2}{2\chi_{||}} \quad ; \quad \tau_{\chi,\perp} = \frac{l_\perp^2}{2\chi_\perp}$$
$$\tau_S = 2 \cdot \left|\frac{\partial S}{\partial U}\right|^{-1} \quad ;$$

$v_{\|\|}$	:	flow velocity along field lines
$c_s = \sqrt{\frac{5(T_i+T_e)}{3m_i}}$	:	sound velocity of the ions
$D_\perp$	:	particle diffusion coefficient perpendicular to the field lines;
$\chi_{\|\|}$, $\chi_\perp$	:	diffusion coefficients parallel and perpendicular to the field lines; (viscosity for momentum equation, heat conductivity for energy equation)
$\frac{\partial S}{\partial U}$	:	derivation of the source term S_U with respect to the variable (flowing quantity) U

A sufficiently good and stable approximation of formula (3.14) is given by the expression:

$$\Delta t_{ion} \leq \left[\tau_{conv}^{-1} + \tau_{D,\perp}^{-1} + \tau_{\chi,\|\|}^{-1} + \tau_{\chi,\perp}^{-1} + \tau_S^{-1}\right]^{-1} \tag{3.15}$$

Remark: The overall timestep for the relaxation of momentum and ion energy has to be chosen as the minimum of all timesteps determined for the propagation of momentum or ion temperature in each cell.

Timestep for the electron species: The additional energy equation for the electrons is of the same form as equation (3.13) but the parallel diffusion coefficient is by a factor of $0.58 \cdot \sqrt{\frac{m_i}{m_e}} \approx 25 \cdot \sqrt{\mu}$ [9] larger than it is for the ion species. Accordingly the electron-energy relaxation time Δt_{el} is much smaller than Δt_{ion} and therefore Δt_{el} should be used to guarantee numerical stability.

But this would require about $10^6 - 10^7$ timesteps to get into a stationary solution. To accelerate the convergence and to save computer time the following numerical procedure has been developed [11]:
The praedictor-step with the characteristic time $\frac{\Delta t_{ion}}{2}$ is applied to the equations for density, momentum and ion energy. Using the corrected values (density, flow velocity, ion temperature and ion pressure) the electron energy equation is solved iteratively on the timescale Δt_{el}. The number of iterations is determined for each ion-timestep as $N_{it} = int(\frac{\Delta t_{ion}}{\Delta t_{el}})$.
After a recalculation of the electron-pressure gradient and the energy exchange term the corrector-step is carried out with timestep Δt_{ion}.

The influence of the flux limits on Δt_{ion} and on Δt_{el} : Since the plasma in the SOL ist not everywhere collision-dominated (see also section 2.4.1), the classical Braginskij-form describing the diffusive transport of momentum and energy (ions, electrons) will lead to unphysically high fluxes (larger than the collision-free values). A rather simple modification of the formulation will avoid this:

[9] $\mu = \frac{m_i}{m_p}$

$$\Gamma_{\chi,\|}^{FL} = \chi_{\|,U}^{FL}\frac{\partial U}{\partial x} = \frac{\chi_{\|,U}^{class}}{1+\left|\frac{\chi\frac{\partial U}{\partial x}}{F_U\cdot\Gamma_{max}}\right|}\cdot\frac{\partial U}{\partial x} \leq F_U\cdot\Gamma_{max} \tag{3.16}$$

Remarks:

- The factors F_U ($U = v_\|, T_i, T_e$) have to be adjusted, to fit the results of kinetic calcultations [12].

variable U	F_U	Γ_{max}
$v_\|$	0.4	$c_s \cdot c_s$
T_i	0.2	$c_s \cdot T_i$
T_e	0.2	$v_{max} \cdot T_e$

- It is still an open question, whether the electrons can exchange information with their thermal velocity ($\Gamma_{max}^e = v_{th}^e \cdot T_e$) or if they are tied to the ions on a microscopic lengthscale (λ_{Debye}) via an electric field, so that the maximal flow velocity is the sound velocity of the plasma ($\Gamma_{max}^e = c_s \cdot T_e$).

- The functional dependency

$$\Gamma_{\chi,\|}^{FL} = \frac{\Gamma_{\chi,\|}}{1+\left|\frac{\Gamma_{\chi,\|}}{F_U\cdot\Gamma_{max}}\right|} \tag{3.17}$$

  is adapted to experimental results, obtained for different collision frequencies in a neutral gas.

- A non-local formulation has been derived, which takes into account all fluxes within a certain distance from the considered point. But the implementation of these effects into the existing SOL-codes is difficult and has only be worked out for special configurations.

In formula (3.14) $\tau_{\chi,\|}$ has to be replaced by $\tau_{\chi,\|}^{FL} = \frac{l_\|^2}{2\chi_\|^{FL}}$. Since $\Gamma_{\chi,\|} \geq \Gamma_{\chi,\|}^{FL}$ and thereby $\tau_{\chi,\|} \leq \tau_{\chi,\|}^{FL}$ the maximal possible timestep is larger after the introduction of flux limits.

Solution in the spatial coordinates

The triangles are only "roughly" orientated to the magnetic field (see section 3.5.1) but the global coordinates are transformed into local coordinates exactly aligned to $\vec{B}$.
The solution of the fluid equations in each cell and for each variable (density, poloidal momentum, radial momentum, ion energy and electron energy) is carried out in these local coordinates. Linear functions are used for interpolating and weighting the variables (Galerkin-approach). Thereby the integration procedure is simplified and all integrals can be solved analytically. The evolution of the variables in time is calculated using the two-step scheme described in the last section.

A detailed analysis of the procedure shows that in the praedictor-step the convective fluxes and source contributions from the nodes in each cell are summed up to give an element-averaged flux. In the corrector-step a complete flux balance – including the diffusive fluxes – is set up between adjacent grid points. This can be interpreted geometrically as a flux exchange along the element sides connecting the nodes.

Treatment of nonlinear terms and source terms

The convection-conduction equations for the variables (density, parallel momentum, ion energy and electron energy) are solved assuming constant flow velocity as well as cell averaged transport coefficients and source terms. Numerical instabilities are prevented through the praedictor-corrector scheme and by the correct choice of the timestep:
Compression effects – variations of pressure because of high convective fluxes of particles and energy – are taken into account trough a recalculation of the variables after the praedictor-step. This treatment is equivalent to the solution of a pressure-correction equation used in the time-implicit method.
The spatial variation of the viscosity and heat conductivity parallel to the magnetic field has to be considered in the computation of the diffusive fluxes. Thereby not only derivatives with respect to the variables but also with respect to the transport coefficients χ^{FL} occur:

$$\frac{\partial}{\partial x}\left(\chi_{\|}^{FL}\frac{\partial U}{\partial x}\right) = \frac{\partial \chi_{\|}^{FL}}{\partial x}\frac{\partial U}{\partial x} + \chi_{\|}^{FL}\frac{\partial^2 U}{\partial x^2} \approx \frac{\Delta\chi_{\|}^{FL}}{l_{\|}}\frac{\Delta U}{l_{\|}} + (\chi_{\|}^{FL})\frac{2\Delta U}{l_{\|}^2} \tag{3.18}$$

Rearranging the two terms one sees that a new and further reduced relaxation time $\tau^*_{\chi,\|}$ has to be introduced:

$$\Delta U\frac{2\chi_{\|}^{FL}}{l_{\|}^2}\left(1+\frac{\Delta\chi_{\|}^{FL}}{2\chi_{\|}^{FL}}\right) = \Delta U\frac{1+\frac{\Delta\chi_{\|}^{FL}}{2\chi_{\|}^{FL}}}{\tau_{\chi,\|}} = \frac{\Delta U}{\tau^*_{\chi,\|}} \tag{3.19}$$

As the evalutation of $\frac{\Delta\chi}{2\chi}$ between adjacent grid points is numerically easy, this nonlinear effect can be taken into account in equation (3.15).
The source terms can be decomposed into contributions from different processes:
- Interactions between electrons and ions
- Interactions between the plasma and neutral particles and/or impurities.

The terms describing the exchange of momentum and energy between the pure-plasma species are only depending on the plasma parameters (density, temperatures of ions and electrons) itself. New values for the sources are calculated after each timestep and an adaption of the size of this step will guarantee stability.
The terms considering the collisions and reactions of the plasma with the neutral particles or impurities are evaluated "externally": an external subroutine or another code are used to determine the rates of production or annihilation of particles, momentum and energy (see chapter 4). Since a complete recalculation of these terms after each timestep requires too much computer time, their spatial distribution is assumed to be constant for many (10 - 100) iterations. Only the source strength is modified in each

iteration and linearly expanded with respect to the plasma flux onto the targets. [10] Nonlinear effects, especially the strong dependence of the reaction rates on the electron temperature, are not taken into account.

3.6 Comparison of the numerical methods used in EB2 and SAFE

3.6.1 The spatial discretization

In both codes the general coordinates are transformed into coordinates along and perpendicular to the magnetic field by an interpolation procedure based on a previously determined magnetic equilibrium. The great advantage of the FEM (SAFE) over the FVM (EB2) is the use of an unstructured grid. Thereby complex boundaries and not-simply connected regions can be discretized in a much more easier way. On the other hand the unstructured discretization lead to an non-regular numbering of the nodes and subsequently to a band shaped "mass-matrix". The inversion of such a matrix needs more computer time than the inversion of a regularly filled matrix, created by the FVM. But one should realize, that in geometrical configurations with "blocked-off" regions or implicitly coupled cut cells this regularity of the FVM-matrices is destroyed and the same algorithms for FEM and FVM must be applied.

3.6.2 The solution procedure

Explicit time marching scheme versus implicit solution

Although the timesteps in the explicit scheme are by a factor of $10 - 20$ smaller than in the implicit procedure this is no major drawback from the computational point of view. The explicit calculation is accelerated by about the same factor by the simpler data structures (no matrix storaging) as well as by the less complex mathematical operations (no matrix inversion).
This argument is still valid for the equation system of ions and electrons, when the special relaxation procedure for the electrons (section 3.5.2) is used. Including the pressure corrections for each node and timestep 17 equations must be solved for the ions, whereas the relaxation of the electron energy equation requires – depending on the flux-limit-factor – between (1-20) iterations. So less than twice the computer time is needed compared to the pure ion-case. Moreover the computer time is increased by only a factor of 1.6 , when the typical flux limits derived in section (3.5.2) are used.
From the physical point of view, the implicit solution procedure seems to be the better alternative, because calculation errors – like numerical diffusion – are not scaling with the simulated time but with the number of iterations. Especially in the electron energy equation instabilities may occur, when a lot of iterations are necessary per ion timestep (explicit scheme).

[10] The variation of this flux is used to decide at which iteration completely new source terms should be determined

Indeed instabilities are induced not only by numerical errors, but also by the nonlinerar energy exchange terms between ions and electrons, which behave like constant external sources on the electron-timescale. If these sources are too large, it may happen that within one ion-timestep the electron-temperature is strongly increased or decreased and no converging time evolution can be found (see also Appendix B).
Such convergence problems can be avoided using a common timestep for electrons and ions (implicit scheme) and a relaxation procedure for the total energy equation (EB2). Thereby an artificially strong coupling between the two species is created and both energy balances (ions, electrons) are strictly fulfilled.
But the question remains, if such a numerical procedure, mainly introduced to overcome the stiffness of the differential equations, is physically meaningful. It has still to be shown – on the electron-timescale – that not only a stationary solution can be found, but also that there is a way in the phase space to get from an initial state into this final state.

Treatment of nonlinearities in transport coefficients and sources

Applying the commonly used flux limits the ion transport is convection dominated and diffusive fluxes play only a minor role, so that changes in these fluxes because of changes in the transport coefficients can be neglected. Therefore in EB2 as well as in SAFE the ion transport coefficients can be approximated as constants in each cell and for each timestep.
The numerical treatment is quite different for the electrons. Whereas in EB2 the heat-conductivity is assumed to be constant, the value is recalculated for each electron-iteration in SAFE. The more accurate approximation within the FE-code has no advantage, if only a stationary solution should be determined; but corrections of the transport coefficients must be considered – even in EB2 – for time-dependent calculations.

In both codes the source terms generated by neutral particles are expanded linearly with respect to the neutral density $\mathbf{n_0}$ in each cell. Since $\mathbf{n_0}$ is proportional to the plasma flux onto the targets, the strength of the source terms is scaled with this flux and corrected after each timestep or iteration. (For further discussion see next chapter)
In addition to that in EB2 the strongly nonlinear variation of the reaction rate is linearized in the electron temperature. This expansion – applied in each cell – is characteristic for an implicit solution procedure and guarantees numerical stability even for an extended timestep. Using an explicit time-marching-scheme this stability is achieved through the adaption of the local timestep. So one can conclude that both schemes are numerically stable on their specific timescales.
Nevertheless for the same configuration global convergence problems may occur in the SAFE-code, while in EB2 a well defined solution is reached. To understand the different behaviour, one has to look in detail into the numerical procedures.
In the EB2-code a large timestep is used, so that an information exchange over a large region is possible and a global flux balance is fulfilled. This means that after each iteration and at a certain time t_n the plasma flux from the inner boundary, the plasma

flux to the target and also the particle sources (generated by the plasma flux) are in an equilibrium and so non-local interactions between the plasma and the neutrals are included automatically.
The situation is quite different in the SAFE-code. Whereas for the plasma a time dependent equation with a small timestep is solved, the distribution of the neutral particles is evaluated in a nearly time-independent approach. Hence for the plasma the transport length within each timestep is at most the length of a grid cell. Only within this distance an information exchange is physically meaningful and only a "local" balance between convection, conduction and sources is fulfilled. To reach a "global" equilibrium many timesteps are necessary, not only to adapt the source- distribution to the changed plasma conditions, but also to bring information from inside of the calculation domain to the walls and thereby get new values for the fluxes of plasma-particles and neutrals. It can be concluded, that as the sources and sinks are instantaneously varying with changes of the plasma state at the walls, the solution is strongly coupled to the wall conditions but only weakly coupled to the plasma state inside of the geometry.
To illustrate this effect a simple one-dimensional energy equation can be solved analytically for the approach described above (see Appendix B). Although in most cases stable solutions exist, the time evolution shows instabilities ($T \leq 0$) inside the calculation domain even for strongly localized recycling.

Chapter 4

Source term calculation in the SAFE-code

The plasma particles (electrons, ions), which hit wall structures recombine inside the target near the surface. The so created neutral particles are emitted into the volume in front of the wall. A part of them is lost in vacuum chambers or through pumping channels. The rest gets into contact with the plasma. Through collisions with electrons and ions momentum and energy are exchanged. Finally the neutral particles are reionized and give contributions to the plasma density. These processes – taken into account in the plasma model-equations as sources and sinks – strongly influence the plasma behaviour in front of the target plates and therefore a physically realistic simulation is important.
In this chapter two models are presented, which can be applied in the SAFE-code. The first model is based on a finite-element solution of a time-independent convection-reaction equation for the neutral particles. The second model simulates the flow of particles and their interactions with the plasma numerically using the Monte-Carlo-technique. The code EIRENE [13] takes into account a large number of interaction processes (charge exchange, elastic/inelastic collisions, reionization etc.) and thereby needs a lot of computer time so that the sources and sinks cannot be recalculated after each plasma-timestep.
Both models are commonly used in SAFE-calculations. First the faster FEM-model is applied to get a sufficiently good approximation of the distributions of particles, temperatures and fluxes.
Then the more time consuming EIRENE-code is iteratively coupled to SAFE to find the final solution.

4.1 FEM-calculation of the source terms

In this model two groups of neutrals are considered, one with a Franck-Condon energy of 3 eV and the other with thermal energy.

For both species the convection-reaction equation

$$U_0 \cdot \frac{\partial n_0}{\partial X} + V_0 \cdot \frac{\partial n_0}{\partial Y} = S_{n0} \tag{4.1}$$

is solved on a triangular mesh, where each side of a triangle (length l in the poloidal plane) is representing a surface $A = 2\pi R \cdot l$.

$X; Y$	:	General coordinates
$W_0 = \sqrt{U_0^2 + V_0^2} = \sqrt{\frac{\gamma T_0}{M_0}}$	:	Thermal velocity of the considered species (factor γ is depending on the distribution function in velocity space)
$S_{n0} = -n_0 n_e \langle \sigma v \rangle_{ion} + S_{wall}$	:	Sinks inside the plasma due to reionization and Sources at the walls

The reaction rate $\langle \sigma v \rangle_{ion}$ takes into account processes due to charge exchange and reionization. A complex formula derived by Janev [14] is used, which strongly depends on the electron-temperature. The source term S_{wall} includes not only the target sources, where the neutrals are emitted initially, but also the sources at the sourrounding walls, where different reflection and absorption processes occur. This treatment is necessary, since it is not yet clear which boundary conditions (for the differential equation) are equivalent to specific reflection and absorption models.
For the FEM-solution the governing equation (4.1) is integrated over the calculation domain applying the Galerkin-method with linear interpolation-functions (N_{ij}; cell index i, node index j). To take into account the complex wall models, the differential equation is solved for each boundary source separately. The complete solution is found afterwards by linear superposition of all individual solutions.

For each of these individual solutions the numerical procedure can be decomposed into several steps and interpreted geometrically :

- A wall source $S_{wall} = \Gamma_{in}$ is calculated for a specific reflection model by integration over the corresponding velocity distribution and angular distribution and by integration over the emitting surface A_1 (represented by side 1 of the triangle) [1] .

  The equivalent equation in the FEM-scheme is:
  $\Gamma_{in} = \int (n_0 \vec{W}_0 d\vec{A}_1) = n_0 \vec{W}_0 \vec{A}_1$

- This flux Γ_{in} enters into a cell of Volume V and creates a neutral density $n_0 = \frac{\Gamma_{in}}{(\vec{W}_0 \vec{A}_1)}$ which is then used to determine the particle flux S_{ion} reionized in this cell.

  The equivalent equation in the FEM-scheme is:
  $S_{ion} = -\int n_0 n_e \langle \sigma v \rangle_{ion} dV$

[1] $[\Gamma_{in}] = \frac{\#}{sec}$

- The remaining flux $\Gamma_r = \Gamma_{in} - S_{ion}$ is divided up into the fluxes Γ_{r1} and Γ_{r2} flowing out of the cell trough the two areas A_2 and A_3 (represented by side 2 and 3 of the triangle) opposite to A_1.

  The equivalent equations in the FEM-scheme are:

  $$\Gamma_{r2} = \int n_{0r}(U_0 \frac{\partial N_2}{\partial x} + V_0 \frac{\partial N_2}{\partial y})dV = n_{0r}\vec{W}_0\vec{A}_2$$
  $$\Gamma_{r3} = \int n_{0r}(U_0 \frac{\partial N_3}{\partial x} + V_0 \frac{\partial N_3}{\partial y})dV = n_{0r}\vec{W}_0\vec{A}_3$$

The last two steps are repeated for the adjacent cells, where now A_2 and A_3 respectively are the inflow-surfaces.

Remark: The developed numerical procedure is equivalent to a volume integrated Monte-Carlo-algorithm for particles with a fixed velocity $\vec{W}_0$. Compared to a MC-code, where a large number of particles have to be started from each wall section to reduce the statistical error, the algorithm derived above approximates the motion of the individual particles by an averaged flux. From this point of view it's evident that the FEM-approach needs about 50 $msec$ computer time, whereas MC-calculations require more than 1 sec.

The computer-time for the simple FEM-model can be further reduced, when a cut-off-condition is introduced. Following the "bunches" of particles through the mesh one arrives at a cell, where only a negligible part of the initial flux is not reionized. If this part is smaller than a given factor F_{cutoff} ($F_{cutoff} \ll 1$) the procedure is stopped. To guarantee particle conservation all source terms $S_{ion}(I)$ (cell number I) determined up to this step are rescaled:

$$S^{eff}_{ion}(I) = \frac{S_{ion}}{1-F_{cutoff}} \qquad \sum_{I=1}^{Ncell} S^{eff}_{ion}(I) = S_{wall}$$

Compared to physically more realistic Monte-Carlo-calculations (see next section) the distribution of the particle sources is approximated very well [1]. Sources of momentum and energy are determined without solving separate differential equations. Instead of this the rather crude assumptions are made:

- momentum sources are neglected:
  $S_{mo} = 0$

- per reionized neutral an energy of $3\,eV$ is tranferred to the ions and for the electrons an energy loss of $25\,eV$ is assumed:
  $S_{E,ion} = S_{n0} \cdot 3\,eV$
  $S_{E,el} = -S_{n0} \cdot 25\,eV$

Exchange of momentum or energy trough inelastic collision processes and non-local effects cannot be described in this simple model. Such interactions, especially important in dense and cool plasmas, are only included in kinetic model calculations.

4.2 Monte-Carlo-calculation of the source terms

Kinetic transport equations (Boltzmann-equation, Fokker-Planck-equation) can be solved using the Monte-Carlo-technique. In this statistical approach the motion and interaction of particles is simulated not only in time and real space, but also in the velocity space. Results of such calculations can be included in a fluid model by integration over the variables.
EIRENE is a widely used Monte-Carlo-code to describe the interaction of neutral particles with a given background plasma [13]. Originally developed to find a time-independent solution, the code has been extended to run in a time-dependent mode. But this extension is still in progress and until now only the time-independent version has been coupled to SAFE.
Since the algorithm and the physical background of EIRENE is intensively described elsewhere [13] the following considerations will concentrate on the numerical procedure which couples the codes each to each other. Starting point of the analyses is a certain plasma state found by the SAFE-code using the simple FEM-neutral-model. Besides the plasma parameters - determined at the center of each element and on the outflow boundaries - a special element-node-file (ELNO-file) is transferred to EIRENE. This ELNO-file includes for each triangle

- the general node numbers of the corners of the cell,
- the coordinates of these nodes,
- the element numbers of the cells adjacent to the three sides and
- a number describing special properties of the sides (emitting, reflecting, absorbing neutral particles or transparent)

At first the informations at the outflow-boundary-cells are evaluated in EIRENE. The plasma flux is integrated over the cell surface and multiplied with a given reflection coefficient characterizing the loss of particles due to pumping. Thereby the flux of neutral particles back into the plasma is determined. Then a number of particles representing these neutrals are started from the target surface. Their motion from cell to cell (geometrical informations from the ELNO-file) and their interactions with the plasma inside each element (physical informations from the plasma file) are simulated using the statistical MC-method. Along the way up to the point where a particle is lost (pumping or reionization) the exchange of momentum and energy is storaged elementwise. The contributions from each particle are scaled with the appopriate flux and the resulting element-integrated source-terms are summed up.

These sources/sinks of particles, momentum and energy can be used in SAFE directly as volume-integrated values in the praedictor-step. For the corrector-step a linear interpolation procedure is necessary to transfer the information from the cell centers to the nodes in a conservative form. After each ion-timestep the source-strength is adapted to the new values of the plasma flux onto the targets, whereas the spatial distribution of the sources remains constant.

Remark: Since certain target regions are physically or geometrically decoupled and the plasma-sources do not influence each other it is common and helpful to define each of these regions as a separate neutral-source. Thereby the flux-rescaling is physically more realistic and the convergence of the code is accelerated.

A new EIRENE-run is necessary, when the background plasma and also the spatial source distribution show considerable changes. The simplest criterium for this decision is the change in the plasma flux onto one of the targets. If the flux has changed by more than a given factor, EIRENE is called again. Moreover the flux-variation is a criterium for the stationarity of the solution: the plasma flux must be constant for a timescale which is large compared to the characteristic transport time. Iterations between EIRENE and SAFE are necessary until this condition is fulfilled.

Chapter 5

Comparison of SAFE-EIRENE and EB2-EIRENE

In this chapter the results of the finite element code SAFE are compared with those of the finite volume code EB2. Both codes are coupled to EIRENE to describe the interaction of the plasma with the neutral particles generated at the targets. As test cases conditions of an ohmic shot of TEXTOR and a discharge in an ASDEX-divertor configuration are chosen.

For the TEXTOR case special care is taken in order to ensure that the same physics are involved for both codes and that the geometrical aspects are comparable as far as possible. In this way the aspects of the different numerical treatments can be isolated and investigated.
The ASDEX-case is chosen mainly to show the applicability of SAFE to a divertor configuration. But a comparison with the results of an EB2-calculation with nearly the same spatial resolution and similar boundary conditions is helpful to relate the numerical procedure to the obtained results.

5.1 Calculation for ohmic conditions in TEXTOR

In a first section the discretization of the scrape-off layer of TEXTOR is presented for the two code systems. Subsequently, the underlying physics model for these simulations is described. In a third section the convergence behaviour of the finite element and the finite volume code is compared. Then, the computed radial profiles in the outer equatorial midplane are discussed and the balances and fluxes are compared.

5.1.1 Geometrical aspects

The calculation domain for this case is the region between a minor radius of 40 cm and a major radius of 50 cm. The flux surface with a minor radius of 46.2 cm is centered at a major radius of 1.75 m. The ALT-limiter is positioned at 44.5 cm and a Shafranov shift of 6 cm at this minor radius is assumed. The magnetic field pitch is obtained by taking the toroidal field to be inversely proportional to the major radius and the reference value is 2.25 T at 1.75 m. The poloidal magnetic field is determined

by a total plasma current of 360 kA and a radial current profile $j(r)$ which inside the separatrix is given by

$$j(r) = j_o(1 - (\frac{r}{a_0})^2)^{q_a} \tag{5.1}$$

with

$$q_a = \frac{2\pi}{\mu_0}\frac{a_0^2}{R_0}\frac{B_0}{I_p} = 5.0\frac{a_0^2}{R_0}\frac{B_0\,(\mathrm{T})}{I_p\,(\mathrm{MA})} \tag{5.2}$$

and j_o is determined from the total plasma current I_p [1, 2]. Outside the separatrix the toroidal current density is assumed to be zero.
Although this geometry can be handled by both codes there still remaine some differences when we look in somewhat more detail into the geometrical aspects.

SAFE-EIRENE

The SAFE code is based on triangle elements oriented parallel and perpendicular to the magnetic surfaces (see Figure 5.1) which can locally be refined in order to resolve steep profiles. However, in the case described here the refinement is chosen such that the size of the elements is comparable with those of the EB2-code. For the EIRENE code the same triangular elements are used.

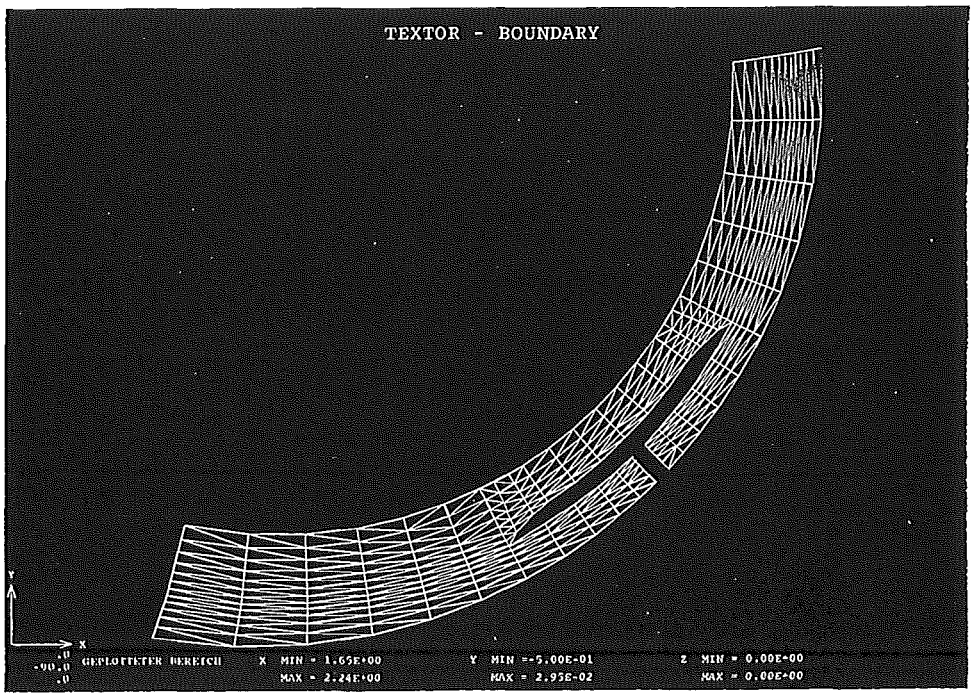

Figure 5.1: Numerical grid of the TEXTOR edge in the vicinity of ALT II (SAFE-EIRENE)

EB2-EIRENE

The EB2 code utilizes an orthogonal curvilinear coordinate system, with one co-ordinate along the magnetic flux surface in the poloidal plane and the second co-ordinate normal to the magnetic flux surfaces. Hence it can explicitly account for the anisotropic behaviour of the plasma. On the other hand this orthogonal curvilinear system limits the choice of the numerical grid because volume elements with orthogonal boundaries have to be chosen. In addition the coding of EB2 – in current versions – is such that local refinements of the grid are not possible.
In order to simulate the ALT-limiter of TEXTOR an orthogonal mesh, aligned with the magnetic flux surfaces, is produced and the volumes corresponding to the interior of the ALT-limiter-blade are then "blocked off". This leads to a mushroom-shaped approximation of the limiter as shown in Figure 5.2. For the EIRENE code the numerical grid is the same as in EB2 with exception of the boundaries which are inclined in order to ensure that the neutral particles are distributed in a more realistic way.
Remark: It should be noted that it is possible to improve the EB2 code such that boundaries inclined with respect to the co-ordinate system can be considered. In this case the second component of the flow crossing the surface has to be written explicitly, whereas the other component can be handled in the normal implicit way. Implementation of this extension is currently carried out.

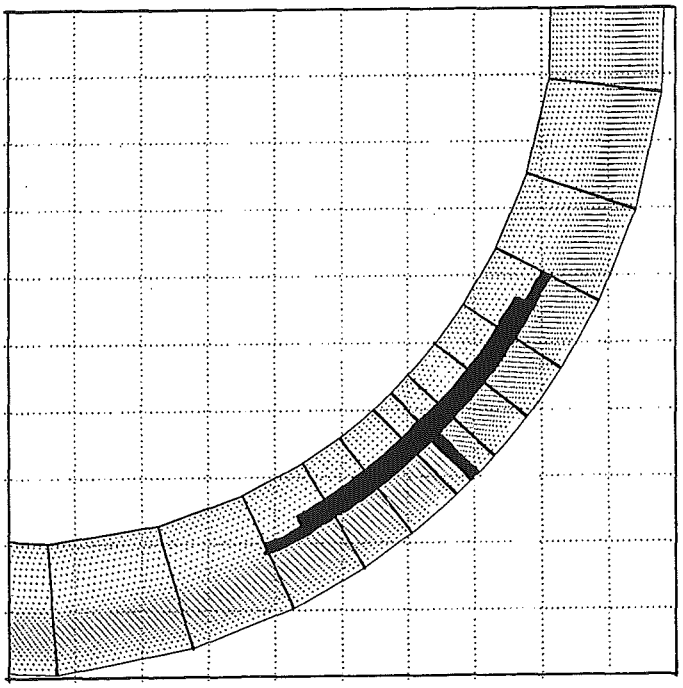

Figure 5.2: Numerical grid of the TEXTOR edge in the vicinity of ALT II (EB2-EIRENE)

5.1.2 Physical model for the TEXTOR-calculation

Equations

In order to simulate a pure hydrogenic plasma ($Z_i = 1$; $n \equiv n_i = n_e$) the five equations are used describing the evolution of plasma density n, the parallel and radial flow velocity components $V_{||}$ and V_r, and electron and ion temperatures T_e and T_i. They are written in an orthogonal coordinate system with one coordinate along the magnetic flux surface in the poloidal cross-section and one co-ordinate normal to the flux surface are used (see equations (2.1) - (2.6)).
The poloidal coefficients are related to the classical parallel coefficients according to $\eta_\theta^i = (B_\theta^2/B^2)\,\eta_{||}^i$, similarly for κ_θ^e and for κ_θ^i. For all these transport coefficients flux limits are introduced (see next subsection).
The radial coefficients are assumed to be anomalous and no inward pinch velocity is taken into account.
The radiation profile is obtained from the experiment. It is poloidally symmetric and the radial dependency is very well described by the following fitting curve :

$$P(r) = \left(1 - \left(\frac{r - r_{max}}{a - r_{max}}\right)^2\right) \cdot P_{max}$$

where :

$P(r)$	:	radiated power in W/m^3	
P_{max}	:	maximum of the radiated power	$(35280\,\frac{W}{m^3})$
r	:	minor radius	$(2r_m - a \leq r \leq a)$
r_{max}	:	minor radius where the profile peaks	$(0.294\,m)$
a	:	minor radius where the profile can be cut off	$(0.440\,m)$

Transport coefficients

The transport coefficients along field lines have been chosen in accordance with present knowledge, i.e. classical coefficients with the commonly used flux limits for the electron heat conductivity, the ion heat conductivity and the parallel ion viscosity (see eq.(3.16)).
The radial transport coefficients (D_r, κ_r^i and κ_r^e) are tuned to match the measurements. The lack of experimental data on poloidal variation of density and temperature profiles, lead in a first approach to the choice of constant transport coefficients in the scrape-off layer instead of Bohm-like or density-scaled coefficients :

$D_r = 0.5\,\frac{m^2}{s}$
$\eta_r = 0.5\,\frac{m^2}{s}$
$\kappa_r^i = 0.2\,\frac{m^2}{s}$
$\kappa_r^e = 0.2\,\frac{m^2}{s}$

Boundary conditions

On the magnetic flux surface at $r = 40cm$, the ion density and electron temperature is prescribed according to the experimental results, the ion temperature is chosen such that the heat flow into the scrape-off layer matches the one which can be estimated from the experimental data. This leads to following boundary conditions :

$n = 1.75 \cdot 10^{19}$ m^{-3}
$u = 0$ m/s
$T_e = 150$ eV
$T_i = 75$ eV

At the limiter, plasma sheath edge conditions are imposed on both sides :

$u_\theta = \frac{B_\theta}{B} u = \frac{B_\theta}{B} c_s$
$Q^e_\theta = 5.5 T_e n V_\theta$
$Q^i_\theta = 3.5 T_i n V_\theta$

At the liner wall (coincident with the flux surface at 50 cm in this model) the boundary conditions are taken from experimental data for n, T_i and T_e :

$n_i = 5 \cdot 10^{17}$ m^{-3}
$T_e = 10$ eV
$T_i = 10$ eV

For the EB2-code isolated cut cells are introduced at a poloidal angle 45 degree below the outermost midplane (i.e. at the limiter position), radially inside the separatrix for particle, momentum and energy flow.
Because of the geometrical flexibility no such constraints are necessary for the SAFE-code.

Neutral modelling

The neutral particles and their interaction with the plasma are simulated by the EIRENE-code. Different reflection-coefficients are chosen for the various target regions. At the limiter tips the neutralized plasma flux is reflected totally ($R_{tips} = 1$), whereas in the scoops 40 % of the flux is lost through the pumping channels ($R_{scoop} = 0.6$). This value has been derived from calculations carried out for the 3-dimensional geometrical configuration of the scoops, the attached vacuum-chambers and the pumps.
The reionized flux Γ^{ion}_{target} is significantly lower than the neutral flux $\Gamma^0 = R \cdot \Gamma^{plasma}_{target}$:

- A fraction of the neutrals coming from the limiter tips leave the calculation domain and penetrate into the core plasma (68 %) :

$$\Gamma^{ion}_{tips} = 0.68 \cdot \Gamma^0_{tips} = 0.68 \cdot R_{tips} \cdot \Gamma^{plasma}_{tips} = 0.68 \cdot \Gamma^{plasma}_{tips}$$

- The situation is quite different for the neutrals generated at the scoop-targets underneath the ALT-II blades: their reionization profile is strongly localized

under the blades of ALT II. The probability for ionization is also reduced because 35 % are deflected back to the target as neutrals (through wall collisions or collisions with the plasma) and can be pumped away :

$$\Gamma^{ion}_{scoop} = 0.65 \cdot \Gamma^{0}_{scoop} = 0.65 \cdot R_{scoop} \cdot \Gamma^{plasma}_{scoop} = 0.39 \cdot \Gamma^{plasma}_{scoop}$$

The source term profiles are determined separately for the neutrals generated at the limiter tips and for the neutrals coming from the scoop-targets. During the plasma-calculation each of the two parts is rescaled with the corresponding plasma flux.
Especially in the TEXTOR-case this partition accelerates the conver gence rate, because the solutions inside and outside of a minor radius of $0.46\,m$ are nearly independent from each other. The fluxes are significantly different ($\Gamma^{plasma}_{tips} \approx 2.5 \cdot \Gamma^{plasma}_{scoop}$) and the interaction between the two regions is nearly negligible. Only 3 % of the neutrals coming from the tips reach plasma surfaces outside the separatrix and influence the solution there. On the other hand the fraction of the neutral flux coming from the scoops and getting inside the separatrix (2 %) causes no significant changes in the balances of particles and energy there.

5.1.3 Convergence behaviour

The first calculations for this TEXTOR-shot are performed with the EB2-code. As mentioned above the transport coefficients are changed until a satisfying agreement with the measured radial profiles is achieved.
These coefficients are then used in the SAFE-code. But with the same physical model no convergent solution for these particular conditions could be found. Even after about 1000 ion-timesteps the electron-temperature profile shows only a weak radial decay, except near the wall where the strongly imposed boundary condition forces the solution to drop from high temperatures ($\sim 150\,eV$) to low temperature ($10\,eV$) enforced near the walls.
This result is physically not meaningful. Hence the SAFE-code was operated in the single-fluid version searching for a stationary solution only for the ion species. The electron temperature has been interpolated from the EB2-solution and was assumed to be constant during the calculation.
For this approach a solution is achieved for the plasma density, for the flow velocities and for the ion temperature.

5.1.4 Comparison of plasma profiles

Ion temperature profile

The profiles obtained for the ion temperature are significantly different between the two codes. Comparing the radial dependency in the outer midplane (see Figure 5.3) the EB2-result shows significant structures, which can be attributed to the energy efflux onto the targets. By this the strong anisotropic transport is reflected: Fast information exchange parallel to the magnetic field lines maintains temperature gradients on a long range which cannot be destroyed by the slow radial diffusion.
In contrast the profile obtained with SAFE is smeared out and of diffusion-like shape. Moreover a shorter decay length of the ion-temperature in poloidal direction is found in the SAFE-calculation.

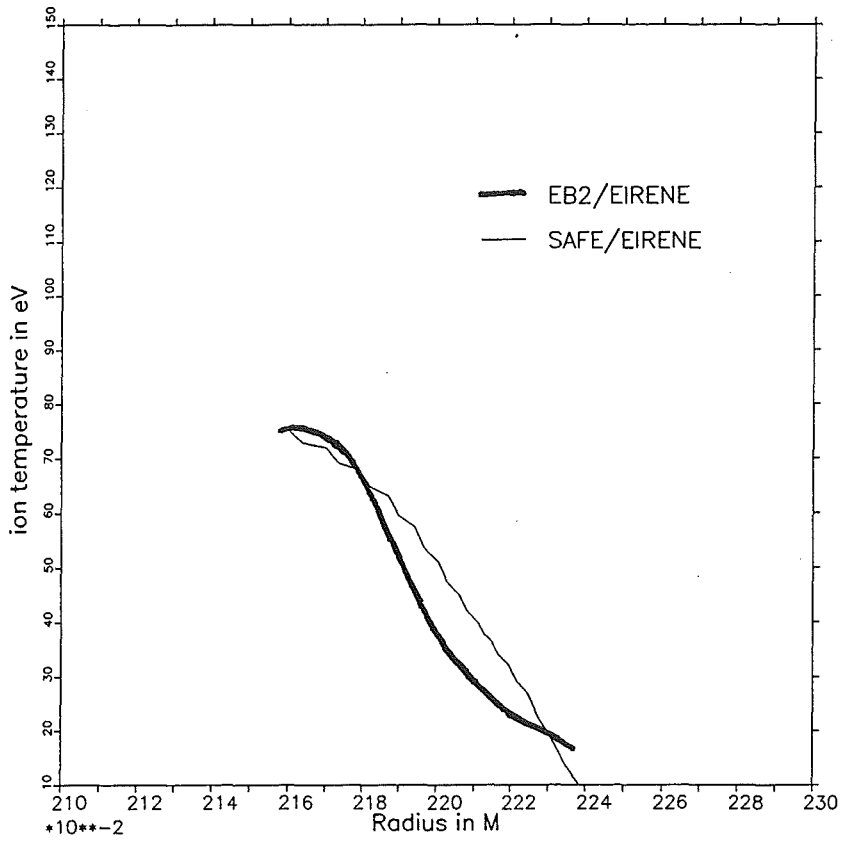

Figure 5.3: radial ion-temperature at the outer midplane of TEXTOR: results from calculations with SAFE-EIRENE and EB2-EIRENE

The different behaviour can be explained by looking in detail into a flux-balance element by element. In the Finite-Volume-formulation parallel transport and radial transport are exactly separated by the special grid structure. Thereby the dissipation-free flux (convection and sound propagation) between adjacent nodes has either a purely parallel component or a purely radial component. Although – especially in the radial coordinate – the connecting line may deviate from the ideal othogonal direction no parallel flux contributions are taken into account in the radial direction.
In contrast to this an element integrated effective flux of the variable U (here: ion temperature T_i) is determined in the FEM-approach. For a certain element (nodes i, j, k) the flux contribution from node j to node i can be separated and is described by the formula (see eq. (3.13) and Appendix A) :

$$\Gamma_{j\to i} = -\int N_j[\,(u + c_s)\frac{\partial N_i}{\partial x} + v\frac{\partial N_i}{\partial y}\,]d\Omega_{el} \cdot U_j$$

u	:	flow velocity in parallel-direction	(x-coordinate)
v	:	flow velocity in radial-direction	(y-coordinate)
c_s	:	sound velocity of the plasma	(derived from the pressure gradient term)

The formula shows that because of the nonperfect orthogonal grid structure one always finds parallel contributions to the flux across magnetic surfaces (points i, j on different magnetic surfaces).
Although this discretization error ("numerical diffusion") has been reduced by stretching the elements in poloidal (parallel) direction ($\|\frac{\partial N_i}{\partial x}\| \approx \frac{1}{10}\|\frac{\partial N_i}{\partial x_\theta}\| \approx \|\frac{1}{100}\frac{\partial N_i}{\partial y}\|$) and aligning them to the magnetic field (deviation less than 5° [1]) ($\|\frac{\partial N_i}{\partial x}\| \approx \frac{1}{1000}\|\frac{\partial N_i}{\partial y}\|$) it cannot be suppressed sufficiently because

- the parallel transport velocity $u + c_s$ is much larger than the radial flow velocity v ($u + c_s \approx 100 \cdot v$) so that $[u + c_s] \cdot \frac{\partial N_i}{\partial x}$ compared to $v \cdot \frac{\partial N_i}{\partial y}$ gives a significant contribution to the effective flux $\Gamma_{j\to i}$.
- the parallel flow velocity is determined by a time-evolution (see eq.(2.2)) whereas the radial flow velocity is calculated "time-independent" from the radial density distribution (see eq.(2.6)) so that numerical diffusion errors of a previous timestep are included implicitly in the actual radial velocity.

Both effects increase the radial fluxes artificially and destroy the nearly one-dimensional flow pattern observed in the FV-calculation. In particular near the target surfaces the stretching factor is reduced, the misalignment to the magnetic field direction is maximal ($\frac{\partial N_i}{\partial x} \approx \frac{1}{200}\frac{\partial N_i}{\partial y}$) and a strong anisotropy in the flow velocity develops. Thereby the contributions of parallel fluxes and radial fluxes are of the same order of magnitude. Consequently the target fluxes are not only fed by transport along field lines but also by artificial fluxes across magnetic surfaces so that a shorter poloidal decay length is sufficient to fulfill the boundary conditions and to sustain a global flux balance.

REMARK :
The preceding discussion explains why a stationary solution for the electron energy equation could not be found. In addition to the convective flow and the sound propagation (pressure gradient force) a faster parallel transport process, i.e. the electron heat conduction, has to be taken into account for the electrons. Applying the commonly used flux limit this diffusive effect can be approximated to first order by an equivalent convective flux $\Gamma^e_{cond} = F_e \cdot v^e_{th} \cdot T_e$ ($F_e = 0.2$). The effective electron energy flux $\Gamma^e_{j\to i}$ can then be written in the form :

$$\Gamma^e_{j\to i} = -\int N_j[\,(u + c_s + F_e \cdot v^e_{th})\frac{\partial N_i}{\partial x} + v\frac{\partial N_i}{\partial y}\,]d\Omega_{el} \cdot [T_e]_j$$

Since

$$F_e \cdot v^e_{th} \approx F_e \cdot \sqrt{\frac{m_{ion}}{m_e}} \cdot c_s \geq 10 \cdot c_s \approx 5000 \cdot v$$

the "numerical diffusion" for the electrons is larger by a factor ten than for the ions. It is even larger than the "real" radial diffusion so that the radial temperature profile is not only disturbed – as it is observed for the ion temperature – but dominated by this artificial flux. This means that no stationary balance between the (poloidally integrated) radial fluxes and the (radially integrated) parallel fluxes can be fulfilled. It should be noted that for a more strongly reduced flux limit, e.g. $\Gamma^e_{cond} \sim c_s \cdot T_e$, stable solutions have been found in a previous work [11].

density profile

The radial density profiles at the outer midplane obtained with EB2 and SAFE are nearly equal (see Figure 5.4). In contradiction to the ion-temperature in the SAFE-result the density is even lower than in the EB2-calculation.

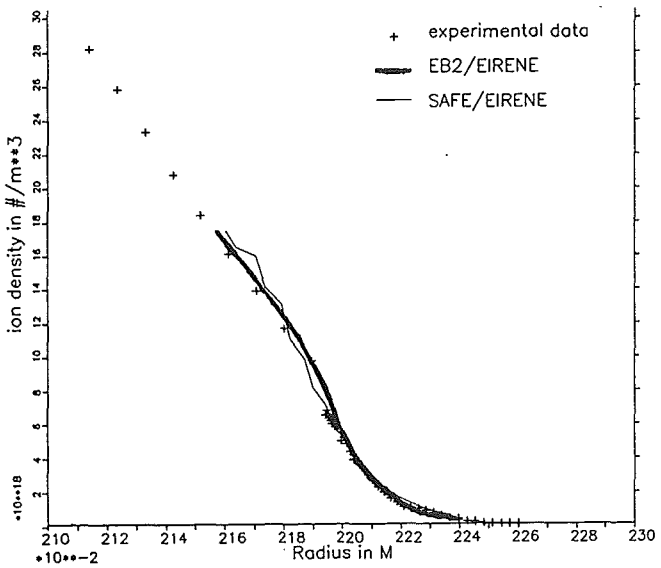

Figure 5.4: radial density profile at the outer midplane of TEXTOR: results from calculations with SAFE-EIRENE and EB2-EIRENE

Mainly two reasons are responsible for this behaviour:

- The profiles agree qualitatively well because the "numerical diffusion" in the continuity equation is less pronounced as in the ion-energy equation. This is evident since in the discretized equation for the particle fluxes only the convective flow velocities – and no sound velocity – occur :

$$\Gamma^n_{j\to i} = -\int N_j[\, u\frac{\partial N_i}{\partial x} + v\frac{\partial N_i}{\partial y}\,]d\Omega_{el} \cdot n_j$$

  Even in regions with low parallel velocity u, e.g. near the symmetry plane the numerical error is negligible.

- The remaining differences between the density distributions are due to an indirect coupling to the wrong ion-temperature profile. The ion-temperature affects the flow velocity u through the pressure gradient force in the parallel momentum equation and through the boundary condition at the target (Bohm-criterium):

$$u_{target} = c_s = (\sqrt{\frac{T_e + T_i}{m_i}})_{target}$$

  Since the ion-temperatures in the SAFE-results are higher and the poloidal decay-length is shorter the plasma particles are accelerated to higher velocities by both the stronger pressure gradient and the higher sound velocity at the targets. This larger particle efflux along the magnetic field has to be equilibrated by a higher radial flux. This leads to the steeper gradients observed in the radial density profile.

5.1.5 Comparison of particle-fluxes and balances

In this subsection the particle-fluxes are compared and the flux balance is checked for both solutions. Therefore the integrated fluxes ($\frac{\#}{s}$) to various surfaces of the calculation domain are evaluated:

Flux $[\frac{\#}{s}]$	EB 2	SAFE	$\Gamma_{EB2}/\Gamma_{SAFE}$
Flux from core	$2.56 \cdot 10^{21}$	$4.38 \cdot 10^{21}$	0.58
Flux to outer wall	$2.52 \cdot 10^{20}$	$2.41 \cdot 10^{20}$	1.04
Flux to limiter-tips	$5.19 \cdot 10^{21}$	$6.97 \cdot 10^{21}$	0.74
Flux to scoop-target	$2.33 \cdot 10^{21}$	$2.84 \cdot 10^{21}$	0.82
Reionized flux	$5.21 \cdot 10^{21}$	$5.83 \cdot 10^{21}$	0.89
Flux balance			
$\lvert\Gamma_{in} - \Gamma_{out}\rvert$	$3.02 \cdot 10^{16}$	$1.59 \cdot 10^{20}$	
$\lvert\Gamma_{in} - \Gamma_{out}\rvert/\Gamma_{in}$	$3.88 \cdot 10^{-6}$	$1.56 \cdot 10^{-2}$	

It is difficult to compare the absolut values of the fluxes, because the ion-temperatures at the targets which have a great influence on the particle flux (Bohm-criterium) are quite different. But some general conclusion can be drawn concerning the physics and special features of the numerical methods.

Although the averaged reionization factor

$$R_{ion} = \frac{\Gamma_{reionized}}{\sum \Gamma_{target}} = \begin{cases} 0.69 & (EB2) \\ 0.59 & (SAFE) \end{cases}$$

is rather low and differs by only 15 % between EB2 and SAFE the flux amplification leads to a 70% higher core-flux in the SAFE-calculation.
Moreover R_{ion} is higher for the EB2-solution than for the SAFE-result which can only be realized by larger neutral losses to the plasma core or back into the pumping channels. Since the electron-temperatures are identical the higher ion-temperatures (SAFE) must favour certain atomic processes so that neutral particles are accelerated or deflected and hence can leave the calculation domain easier. Analysing the reaction-rates one finds that the higher probability for charge exchange processes causes an acceleration (higher neutral velocity) and through elastic collisions with the ions the neutrals are deflected more effectively into the pumping channels.
The exact flux balance shows the advantage of the implicit solution method (EB 2). For each iteration a global flux conservation is guaranteed, whereas the information-exchange between the core-plasma and the targets in the explicit formulation (SAFE) requires a large number of timesteps. Within these steps numerical errors in the local flux-balance cannot be avoided and sum up to give a larger error in the global flux conservation.

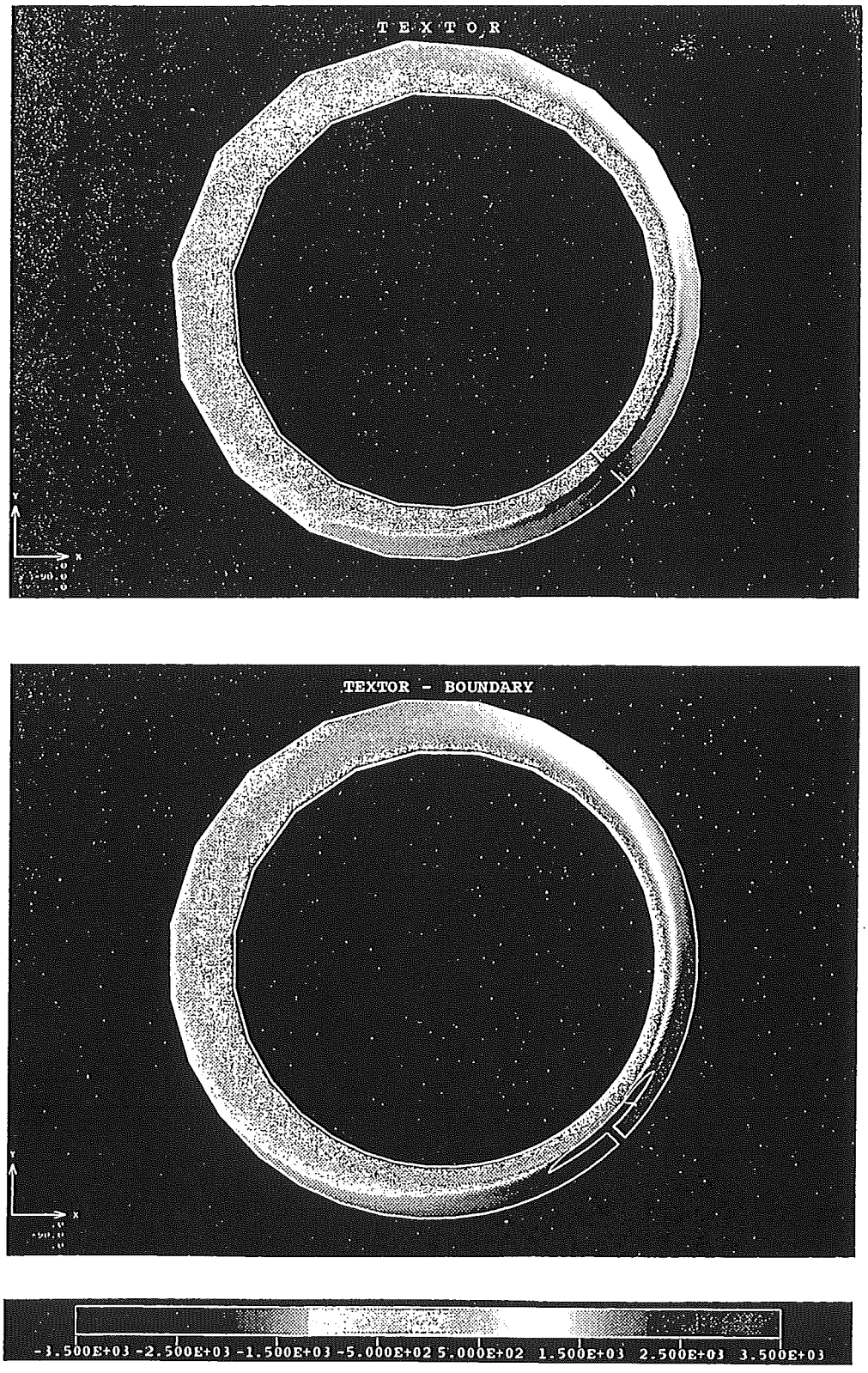

Figure 5.5: poloidal velocity distribution in the edge of TEXTOR: results from calculations with EB2-EIRENE (top) and SAFE-EIRENE (bottom)

5.2 Calculation for the ASDEX-LYRA configuration

The SAFE-EIRENE code has been applied to the ASDEX divertor configuration LYRA. The geometrical data and a converged solution of EB2-EIRENE [15] are used to set up a FEM-mesh with equivalent boundary conditions and to transfer the electron temperature values from the EB2-grid to this mesh. As in the TEXTOR-calculation these values are assumed to be constant during the calculation. The ion-temperature, the flux distribution and the density profiles are determined by SAFE-EIRENE.
From the numerical point of view the main difference compared to the TEXTOR-case is not only the different magnetic configuration but also the different mesh structure.

5.2.1 Geometrical aspects

Figure 5.6 shows the FEM-mesh for the ASDEX-LYRA configuration. Only the region from the outer midplane to the X-point including the outer divertor leg is considered. The generated FEM-mesh is nearly adapted to the magnetic flux surfaces, but it is unstructured: the number of radial cells at the outer midplane is smaller than near the X-point or in front of the target. This means that along the poloidal coordinate additional triangles are inserted to provide a higher spatial resolution.

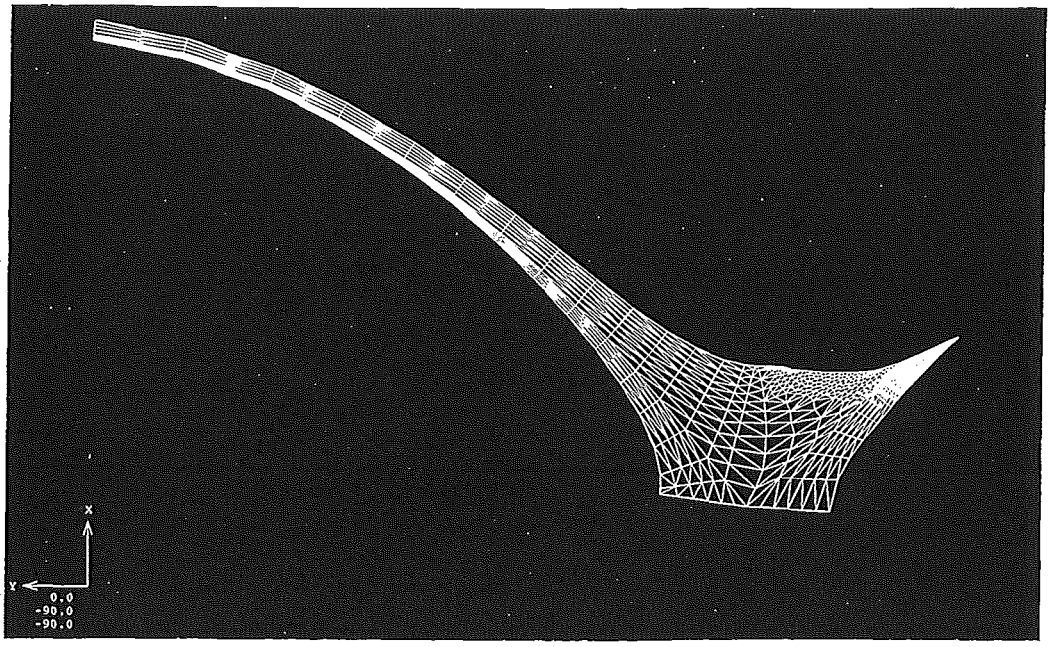

Figure 5.6: FEM-mesh for the simulation of the ASDEX-LYRA configuration with SAFE-EIRENE

5.2.2 Physical model

Equations and transport coefficients

As for the TEXTOR-calculation the commonly adopted model equations (2.1 - 2.6) with the flux-limited parallel transport coefficients are solved. For the radial transport coefficients the following values are used :

$D_r = 0.3 \frac{m^2}{s}$
$\eta_r = 0.2 \frac{m^2}{s}$
$\kappa_r^i = 1.0 \frac{m^2}{s}$
$\kappa_r^e = 1.0 \frac{m^2}{s}$ (not explicitly considered in the SAFE-calculation)

Boundary conditions

The rather complex boundary conditions chosen for the EB2-EIRENE calculation are slightly changed and simplified to save computer time and to take into account the artificially created "cuts" near the midplane and at the X-point [1].
At the core-boundary and at the wall the values for n, u_θ, v, T_i, T_e are taken from the EB2-EIRENE solution and these values remain unchanged during the calculation. These values vary along the boundary, and are approximately :

Core :
$n \sim 1.5 \cdot 10^{20}$ m^{-3}
$u_\theta \sim 0$ m/s
$T_e \sim T_i \sim 90$ eV

Wall :
$n \sim 3 \cdot 10^{19}$ m^{-3}
$T_e \sim T_i \sim 12$ eV

At the target surface the plasma sheath edge conditions are imposed :
$u_\theta = \frac{B_\theta}{B} u = \frac{B_\theta}{B} c_s$
$Q_\theta^e = 5.5 \cdot T_e n V_\theta$
$Q_\theta^i = 3.5 \cdot T_i n V_\theta$
The particle reflection coefficient for the plasma flux onto the target is set to $R = 0.7$ in both codes.

At the outer midplane and at the boundary intersecting the X-point all poloidal gradients are forced to vanish. The radial velocity is taken from the EB2-calculation.

[1] In the EB2-calculation the whole edge plasma with inner divertor and outer divertor is considered

5.2.3 Convergence behaviour

Starting from a linear ion-temperature profile in radial direction, nearly constant ion-temperatures along the field lines and zero flow velocities a stationary solution is reached after 45000 timesteps which is equivalent to a simulated time of $3 \cdot 10^{-2}$ *sec.* For the first 7500 timesteps the FEM-neutral model is used. Then EIRENE is called 9 times until a maximum error of 0.1 % in the relative particle balance is achieved. No temperature instabilities arise because the sources are strongly localized just in front of the divertor target (see Appendix B).
Since the electron-temperature – mainly influenced by the plasma-neutral interactions – is fixed and only the ion-temperature and the particle fluxes have to be adjusted only a few EIRENE-iterations are necessary.

As it has been observed in the TEXTOR-case the radial ion-temperature profile is broadened in the SAFE results as compared to the EB2 case, because of numerical diffusion. Therefore the further discussion concentrates on the flow field and the density distribution, recalling that both agreed qualitatively well in the TEXTOR-application.

5.2.4 Comparison of the velocity distributions

Figure 5.7 shows the poloidal velocities obtained with the EB2-code and the SAFE-code respectively. The following general features are found in both solutions:

- The radially outflowing particles are accelerated in a small jet along the field lines up to supersonic velocities.
- This jet is deflected to the target, so that near the X-point the poloidal velocities are very low.
- Just in front of the target the particles are accelerated once more to fulfill the Bohm-criterium at the divertor surface.

But a detailed analysis of the flow field exposes significant differences. In the EB2-solution the particles flow mainly inside the separatrix and the deflection occurs near the X-point, whereas in the SAFE-result the acceleration begins near the outer mid-plane on flux surfaces outside the separatrix. Thereby a direct connection between the core plasma and the target is established. This different behaviour in the SAFE-calculation is caused by higher radial fluxes in the region where the additional cells are inserted. Since each of these elements violates the requirement of field-alignment the enhanced transport can be explained by numerical diffusion errors.

5.2.5 Comparison of the density distributions

The two density distributions presented in Figure 5.8 confirm the statement that numerical diffusion errors are not sufficiently suppressed in the FEM-solution-scheme. Compared to the EB2-solution, where the particles are strongly tied to the magnetic flux surfaces (nearly constant plasma density along a fixed field line), the SAFE-result shows an enhanced transport across the magnetic surfaces.

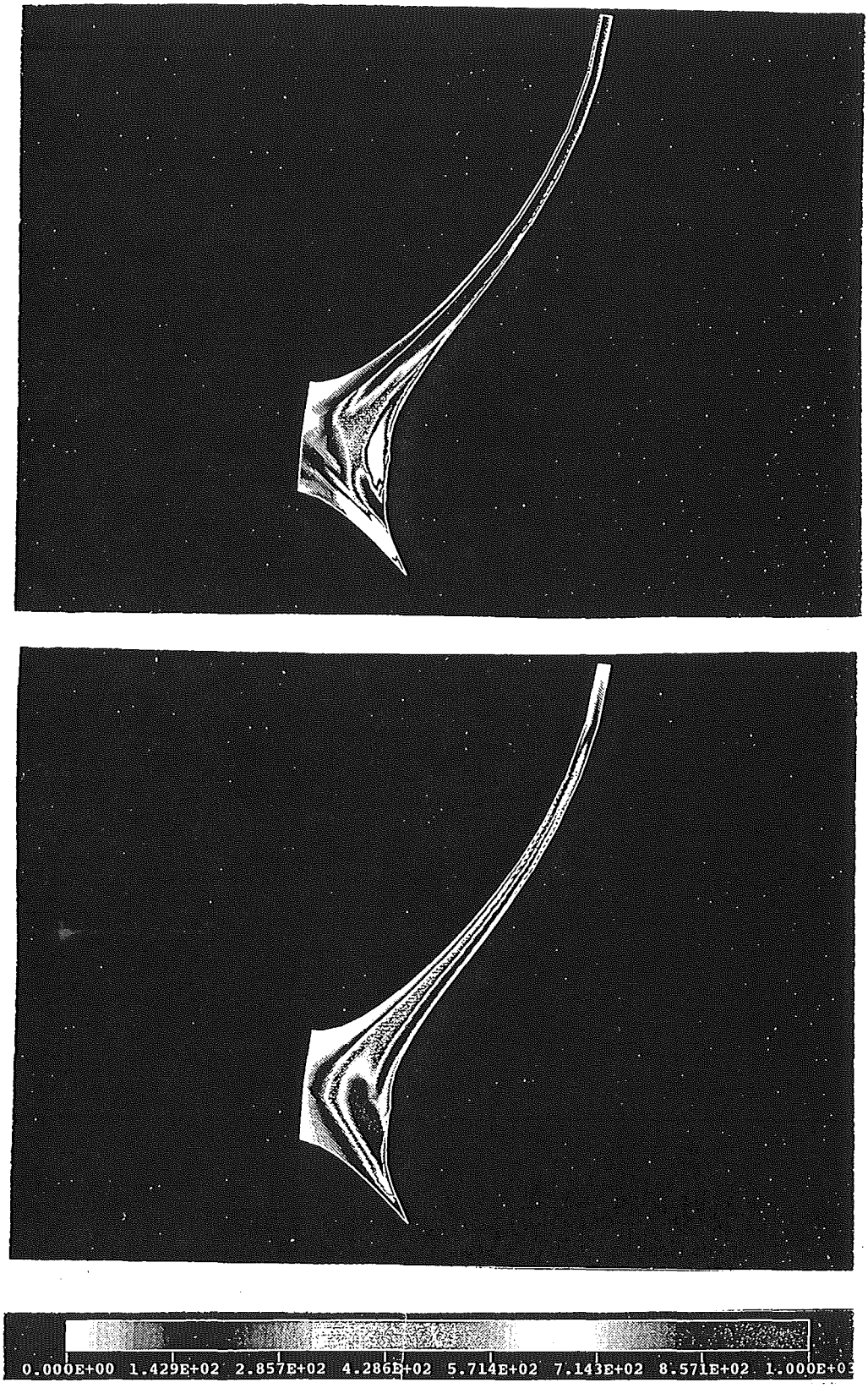

Figure 5.7: Poloidal velocity distribution for the ASDEX-LYRA case: EB2-EIRENE (top); SAFE-EIRENE (bottom)

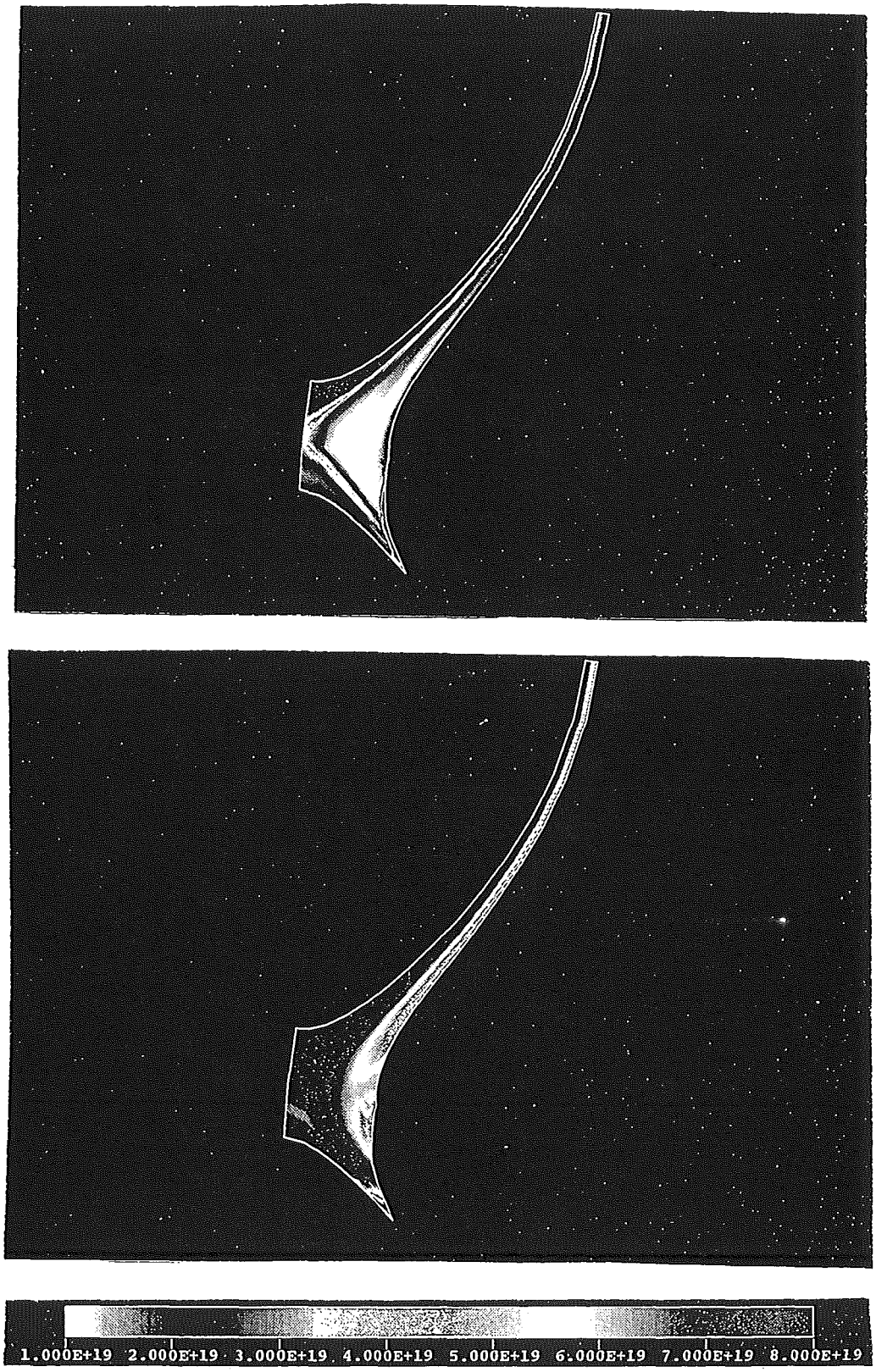

Figure 5.8: density distribution for the ASDEX-LYRA case: EB2-EIRENE (top); SAFE-EIRENE (bottom)

5.2.6 Distribution of the particles sources

The reionization of the neutral particles (see Figure 5.9) takes place in a small region just in front of the divertor target. The decay length of the source profile in parallel direction is of the order of a few centimeters. The assumption of constant source terms in each element therefore requires a large number of rather small cells to provide a sufficient spatial resolution.
Nearly the same accuracy with respect to physical and numerical aspects can be achieved using larger cells but a better interpolation function in each cell. In Appendix C the finite Volume solution-scheme (EB2) is extended to take into account such strongly localized source terms; in each element the sources are approximated by a linear superposition of exponential functions permitting to describe peaked profiles as well as hollow profiles within a cell.

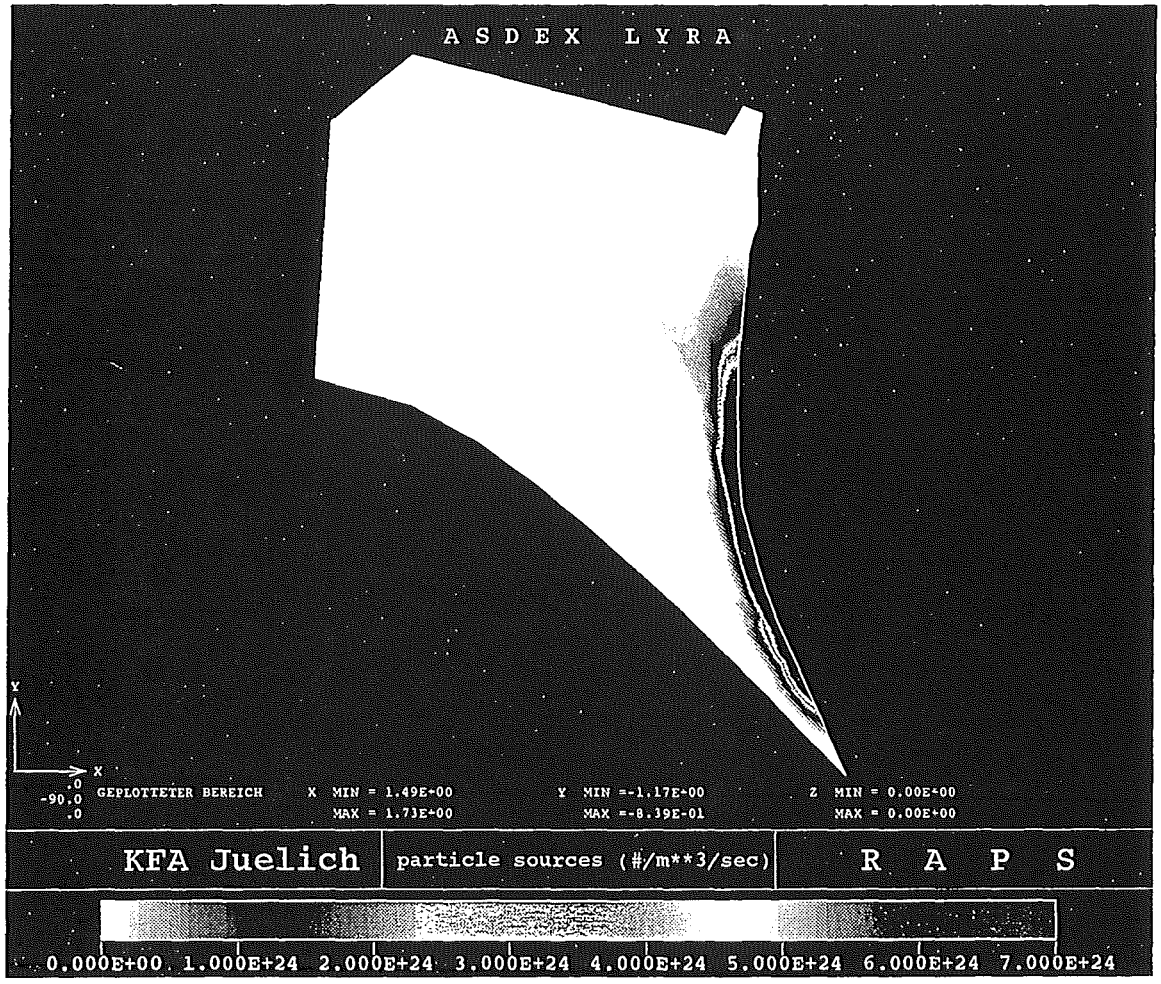

Figure 5.9: particle sources for the ASDEX-LYRA case (SAFE-EIRENE)

Chapter 6

Conclusions

The code systems EB2-EIRENE and SAFE-EIRENE have been developed to compute stationary solutions for the density, the flow velocities and the temperatures of ions and electrons in the SOL of tokamaks.
The Monte-Carlo-code EIRENE is used to describe the transport of neutral particles and their interactions with the plasma in the region considered. SAFE and EB2 are codes, which solve the plasma-fluid-equations at discrete points of the calculation domain by different numerical integration procedures.
Each integration method can be derived from the underlying differential equations using a general formalism, which takes into account the mesh structure and the variation of the solution between adjacent nodes. Characteristic features of the EB2-algorithm (**F**inite-**V**olume- **M**ethod) are the geometrically inefficient orthogonal grid structure with regularly numbered nodes combined with numerically flexible interpolation functions. In Contrast to this the SAFE-algorithm (**F**inite-**E**lement-**M**ethod) is based upon a geometrically flexible triangular mesh with rather crude linear interpolation functions.
Both methods – FVM and FEM – are commonly used to solve fluid equations of Navier-Stokes-type (convection-conduction-equations) in 2-D or even in 3-D. But the applicability to the plasma-fluid equations in the SOL has only been proven for the FVM. Therefore a comparison between EB2 and SAFE is carried out to check the accuracy and the numerical stability of the FEM concerning the special features of the plasma motion.

Anisotropy in transport – Numerical diffusion

A theoretical analysis and especially the comparison of the results of EB2-EIRENE and SAFE-EIRENE show that the FEM with linear interpolation functions creates significant numerical diffusion errors. They are caused by the strongly anisotropic transport velocities parallel to the magnetic field and orthogonal to it. Even a nearly exact alignment of the grid cells to the characteristic directions of transport (deviation less than 5°) cannot suppress this effect sufficiently:

- For the **TEXTOR-case (structured mesh)** the density distribution in the SAFE-calculation is similar to the result obtained with EB2. Nevertheless a

consistent solution cannot be achieved with SAFE because the temperature-profiles of ions and electrons are disturbed by numerical diffusion errors.
Remark: Comparing the characteristic velocities along field lines describing the transport of electron-energy ($v_{th}^e = \sqrt{\frac{T_e}{m_e}}$), the transport of ion-energy ($c_s = \sqrt{\frac{T_i+T_e}{m_i}}$) and the transport of particles ($u \leq c_s \ll v_{th}^e$) it is evident that the density distribution is less affected by numerical diffusion.

- For the **ASDEX-case (unstructured mesh)** one finds totally different results even for the density distribution using EB2 and SAFE respectively. A detailed analysis of the flow field shows that in each radially inserted element large artificial fluxes across magnetic surfaces are created. Since especially these cells are not aligned to the field these fluxes can also be attributed to numerical diffusion effects.

The rather large errors obtained with the time-explicit method are reduced when a time-implicit method is applied [?], but they cannot be avoided since the two-dimensional structure of the interpolation functions is a special feature of the FEM. So it may happen that after a large number of iterations – necessary to take into account the strong nonlinearities in the transport coefficients and in the source terms – even in a time-implicit solution unphysically high radial fluxes occur.

These enhanced fluxes can be suppressed effectively when in addition to the approximate alignment to the characteristic transport directions (along and perpendicular to the magnetic field) solution-dependent interpolation/weighting functions are chosen; in the case of SOL-calculations an exponential interpolation function in radial direction can reduce the information exchange with respect to poloidal transport for mesh points on different magnetic surfaces.
Whether only the adaption of the interpolation functions – without explicit field alignment of the mesh – is sufficient to "decouple" the solutions on different field lines has to be checked in further calculations.

Relaxation of the differential equations – Numerical instabilities

Strong nonlinearities and non-local effects are introduced mainly by the interactions of the plasma with the neutral particles. These sources and sinks of particles, momentum and energy may drive instabilities in the numerical scheme used to solve the plasma-fluid equations. Especially the coupling of a time-explicit solver for the plasma-equations to a time-independent solution method for the neutral distribution (SAFE-EIRENE) can trigger such instabilities.
Their evolution can be explained using an analytical model describing the global fluxes of particles, momentum and energy. Starting point of the analysis is a given plasma state. The density and the temperatures at the target plate combined with a plasma-reflection-coefficient determine the neutral flux back into the SOL. Following the time-independent approach the reionization of the neutrals is instantaneously taken into account in the plasma-equations. Thereby the plasma temperature is significantly reduced in the region where the reionization takes place. But the explicit-time-marching

scheme transmits this information only to adjacent cells so that the temperatures and fluxes at the target remain nearly constant. Therefore in the actual iteration the energy losses are again as high as in the previous timestep. So it may happen that before the conditions at the target are adapted to the new plasma state the electrons in the reionization-zone are cooled down to unphysically low temperatures ($T_e \leq 0$).
The formation of such instabilities can be prevented when in the numerical scheme the flux balance for particles, momentum and energy is fulfilled over a larger spatial domain, which means that a time-implicit solution method with enhanced timestep must be applied.

Suggestions for a HYBRID – SCHEME

Further code development should combine the advantages of each method. – FEM and FVM. From the EB2-code the solution algorithm (Patankar-method) should be retained because it is a robust method applicable to very different physical processes, including strong convection, diffusion and source terms. Moreover the time-implicit treatment can deal adequately with the stiffness of the plama-fluid equations and avoids instabilities generated by plasma-neutral-interactions. A better approximation for the interpolation in time (Newton-method) is easy to introduce in the presently used version of the EB2-code.

For a geometrically flexible treatment in the spatial coordinates the theoretical formalism of the FEM should be used. Instead of the heuristically introduced multiplication of fluxes with corresponding surfaces or the weighting of variables – like density and energy – with discrete volumes (EB2) a general intergration procedure can be applied. The use of an unstructured mesh simplifies the discretization of complex geometries even in not simply connected domains. In addition to that the interpolation functions can be adapted to the physically relevant process, which may change over the calculation domain considered.
For the SOL-calculations a first step has been the implementation of an adequate solution-procedure for spatially strongly varying source terms. The evaluated numerical scheme in particular is useful to accelerate the convergence of divertor-cases with detached solution near the target plates.
All these extensions do not touch the orthogonal grid structure in the calculation domain, which prevents numerical diffusion by definition.

Nevertheless on a longer timescale a FEM-code should be developed in which two-dimensional and solution-adapted interpolation/weighting functions are used so that even in a non-regular and non-orthogonal mesh discretization-errors can be neglected. Although such a code-development is a long-term project and results can be achieved only after years the know-how is still necessary in other fields of plasma-physics and of general interest in numerical physics.

Appendix A

Comparison of FEM and FVM for a 2D-convection-equation

To compare the FEM and the FVM the 2D-convection-equation

$$\dot{\Phi} + \frac{\partial(u \cdot \Phi)}{\partial x} + \frac{\partial(v \cdot \Phi)}{\partial y} = \frac{\partial \Gamma^x}{\partial x} + \frac{\partial \Gamma^y}{\partial y} = 0 \qquad \text{(A.1)}$$

is considered.
The following geometrical configuration is discretized using triangles for the FEM and quadrilaterals for the FVM.

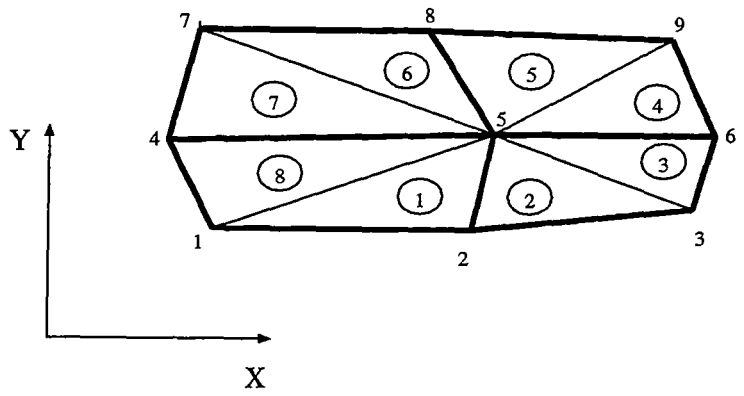

Applying the **FEM integration procedure** one finds for equation (A.1) an equation system for the unknowns $\Phi_k \quad (k = 1....9)$:

$$\sum_{El=1}^{8}\sum_{k=1}^{3}\{\dot{\Phi}_k \int N_j N_k d\Omega_{El}\} = -\sum_{El=1}^{8}\sum_{k=1}^{3}\{\Gamma_k^x \int N_j \frac{\partial N_k}{\partial x} d\Omega_{El} + \Gamma_k^y \int N_j \frac{\partial N_k}{\partial y} d\Omega_{El}\} \qquad \text{(A.2)}$$

Assuming linear weighting and interpolation functions (defined for each element **E**)

$$N_j = a_j + b_j \cdot x + c_j \cdot y \qquad (j = 1,2,3)$$

with the coefficients

$a_j = \frac{x_j y_k - x_k y_j}{2A_E^{\triangle}}$; $b_j = \frac{y_j - y_k}{2A_E^{\triangle}}$; $c_j = \frac{x_k - x_j}{2A_E^{\triangle}}$; $A_E^{\triangle}$: area of the triangle

The right hand side (flux balance) of equation (A.2) can be evaluated especially for the central point **5**.

Flux balance at Point 5:

$$\begin{aligned}
&[\ (y_2 - y_4)\cdot\Gamma_1^x + (y_3 - y_1)\cdot\Gamma_2^x + (y_6 - y_2)\cdot\Gamma_3^x + (y_1 - y_7)\cdot\Gamma_4^x + \\
&\quad (y_9 - y_3)\cdot\Gamma_6^x + (y_4 - y_8)\cdot\Gamma_7^x + (y_7 - y_9)\cdot\Gamma_8^x + (y_8 - y_6)\cdot\Gamma_9^x \\
&+ \\
&\quad (x_4 - y_2)\cdot\Gamma_1^y + (x_1 - x_3)\cdot\Gamma_2^y + (x_2 - x_6)\cdot\Gamma_3^y + (x_7 - x_1)\cdot\Gamma_4^y + \\
&\quad (x_3 - x_9)\cdot\Gamma_6^y + (x_8 - x_4)\cdot\Gamma_7^y + (y_9 - y_7)\cdot\Gamma_8^y + (y_6 - y_8)\cdot\Gamma_9^y \quad] \ \cdot \ -\tfrac{1}{6}
\end{aligned}$$

The flux balance at point 5 can also be written in the following form:

$$\begin{aligned}
&[\ (y_1 - y_2)\cdot\tfrac{\Gamma_1^x+\Gamma_2^x}{2} + (y_2 - y_3)\cdot\tfrac{\Gamma_2^x+\Gamma_3^x}{2} + (y_3 - y_6)\cdot\tfrac{\Gamma_3^x+\Gamma_6^x}{2} + (y_6 - y_9)\cdot\tfrac{\Gamma_6^x+\Gamma_9^x}{2} + \\
&\quad (y_9 - y_8)\cdot\tfrac{\Gamma_8^x+\Gamma_9^x}{2} + (y_8 - y_7)\cdot\tfrac{\Gamma_7^x+\Gamma_8^x}{2} + (y_7 - y_4)\cdot\tfrac{\Gamma_4^x+\Gamma_7^x}{2} + (y_4 - y_1)\cdot\tfrac{\Gamma_1^x+\Gamma_4^x}{2} \\
&+ \\
&\quad (x_2 - x_1)\cdot\tfrac{\Gamma_1^y+\Gamma_2^y}{2} + (x_3 - y_2)\cdot\tfrac{\Gamma_2^y+\Gamma_3^y}{2} + (x_6 - x_3)\cdot\tfrac{\Gamma_3^y+\Gamma_6^y}{2} + (x_9 - y_6)\cdot\tfrac{\Gamma_6^y+\Gamma_9^y}{2} + \\
&\quad (x_8 - y_9)\cdot\tfrac{\Gamma_8^y+\Gamma_9^y}{2} + (x_7 - x_8)\cdot\tfrac{\Gamma_7^y+\Gamma_8^y}{2} + (x_4 - x_7)\cdot\tfrac{\Gamma_4^y+\Gamma_7^y}{2} + (x_1 - x_4)\cdot\tfrac{\Gamma_1^y+\Gamma_4^y}{2} \quad]\cdot\tfrac{1}{3}
\end{aligned}$$

The expression inside the brackets is equivalent to the flux balance obtained with the 9-point-scheme in a finite-volume formulation: all fluxes normal to the sides surrounding the central point are summed up [17].
The factor $\frac{1}{3}$ appears in the FEM on both sides of the discretized convection-equation and thereby cancels out (see **REMARK** below).

Nevertheless the specific integration procedures used for the FEM and the FVM respectively lead to different expressions for the left-hand side of equation (A.2) (Mass matrix **M**). In the FVM approach only the diagonal elements $M_{i,i}$ are different from zero, whereas in the FEM treatment also the non-diagonal matrix-elements $M_{i,j}$ – where the points i and j belong to one cell – are different from zero.
Because of these additional matrix-elements not only adjacent points can exchange fluxes but also a transport of information over a larger distance is realized. One important consequence for conventional (isotropic) fluid simulations is the reduction of numerical diffusion in the FEM compared to the FVM.

REMARK:
The structure of the FEM mass matrix can be artificially simplified by "lumping" the matrix, which means by summing up all elements of each row j of the matrix. This value is then taken as the new diagonal element $M_{j,j}$ while all off-diagonal entries are set to zero. The procedure can be interpreted as an isolated summation over the integrals while the solution only at point j Φ_j is taken into account. Since the relation $\sum_{k=1}^{3} N_k = 1$ is fulfilled for each element the new diagonal matrix-element is:

$$\sum_{El=1}^{8} \{\dot{\Phi}_j (\sum_{k=1}^{3} \int N_j N_k d\Omega_{El})\} = \sum_{El=1}^{8} \{\dot{\Phi}_j (\sum_{k=1}^{3} \int N_j d\Omega_{El}\}$$

$$= \dot{\Phi}_j \cdot \sum_{El=1}^{8} (\frac{1}{3} A_E^{\triangle}) = \dot{\Phi}_j \cdot \sum_{El=1}^{4} (\frac{1}{3} A_E^{\square})$$

Using this approach the FEM and the 9-point FVM are equivalent.

Appendix B

Solution of a 1D-convection-conduction-equation including source terms

Until now in the EB2-code the interpolation functions derived by Patankar [4] are used. These functions are derived from the one-dimensional time-independent convection-conduction equation

$$\rho u \cdot \Phi' = D \cdot \Phi'' \tag{B.1}$$

The solution within one cell ($0 \leq x \leq L$) is given by the formula

$$\Phi = \Phi_0 + (\Phi_L - \Phi_0) \cdot \frac{e^{P\frac{x}{L}} - 1}{e^P - 1} \qquad with \quad P = \frac{\rho u L}{D} \tag{B.2}$$

Assuming flux conservation between adjacent cells an equation is found determining the solution at the central point P (see figure below):

$$a_P \, \Phi_P = a_W \, \Phi_W + a_E \, \Phi_E$$

with the coefficients

$$a_P = (\rho u)_1 \cdot \left[\frac{1}{e^{P_1} - 1}\right] + (\rho u)_2 \cdot \left[\frac{e^{P_2}}{e^{P_2} - 1}\right]$$

$$a_W = (\rho u)_1 \cdot \left[\frac{e^{P_1}}{e^{P_1} - 1}\right]$$

$$a_E = (\rho u)_2 \cdot \left[\frac{1}{e^{P_2} - 1}\right]$$

If moreover a source S is considered in equation (B.1)

$$\rho u \cdot \Phi' = D \cdot \Phi'' + S \tag{B.3}$$

an additional term Q occurs in the equation for Φ_P:

$$a_P \Phi_P = a_W \Phi_W + a_E \Phi_E + Q$$

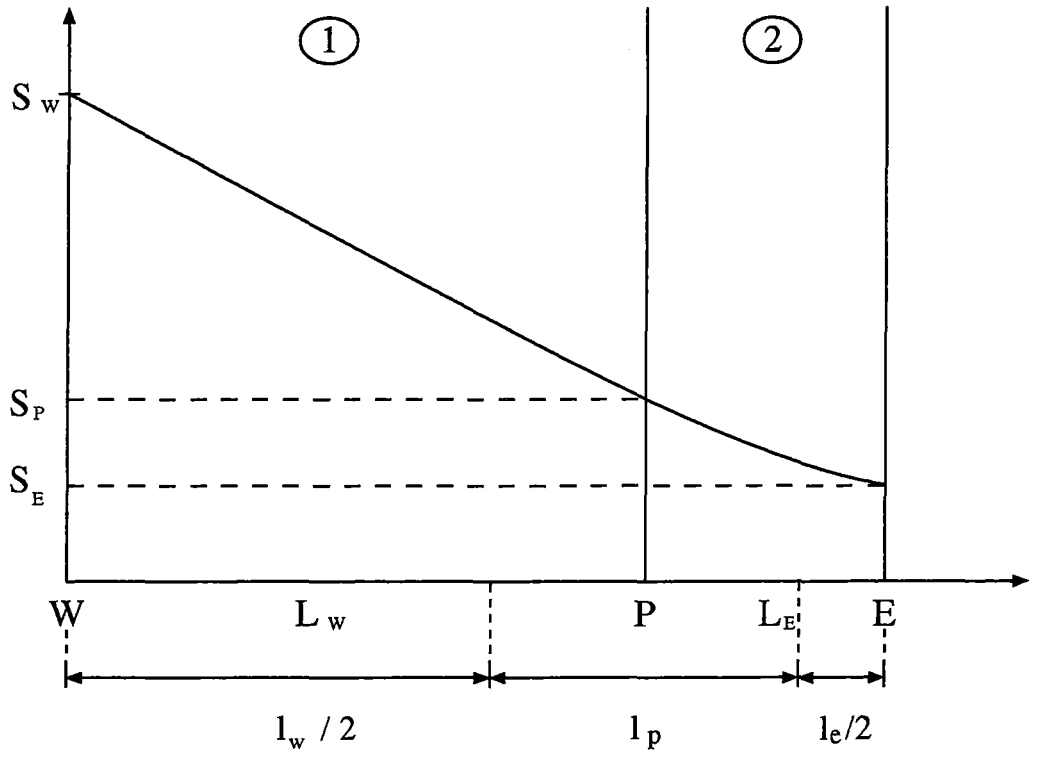

Q can be derived under the assumption of a spatially constant source S located at point P. It has the simple form

$$Q = S_P l_P$$

Such a crude estimation reduces the convergence rate of the numerical scheme in situations where strong spatial gradients occur in the source terms. The scheme can be improved when not only the source strength at point P but also the adjacent source terms S_W and S_E are taken into accout. Proceeding in the same way as Patankar one derives a formula for Q using different interpolation functions between the grid points.

Linear interpolation of the source terms

$$Q = \frac{S_W l_W}{2} \cdot [1 + g(P_1)] + \frac{S_P l_P}{2} \cdot [1 + g(P_1) + g(P_2)] + \frac{S_E l_E}{2} \cdot [-g(P_2)]$$

with $g(P_i) = -\frac{1}{P_i} + \frac{1}{e^{P_i}-1}$

Exponential interpolation of the source terms

$$Q = L \cdot \{S_W F_W + S_P F_P + S_E F_E\}$$

with $L = \frac{L_1+L_2}{2}$; $w = e^{\frac{L_1}{L}}$; $r = e^{\frac{L_2}{L}}$; $N = (rw-1)(w-1)(r-1)$

and

$$F_W = +\frac{w(r-1)}{N} \cdot F_a + \frac{rw(r-1)}{N} \cdot F_b - \frac{w(r^2-1)}{N} \cdot F_c$$

$$F_P = -\frac{w(rw-1)}{N} \cdot F_a - \frac{r(rw-1)}{N} \cdot F_b + \frac{r^2w^2-1}{N} \cdot F_c$$

$$F_E = +\frac{rw(w-1)}{N} \cdot F_a + \frac{r(w-1)}{N} \cdot F_b - \frac{r(w^2-1)}{N} \cdot F_c$$

F_a, F_b and F_c are functions of the Peclet-numbers in the cells and depend on L_1 and L_2:

$$F_a = \frac{LP_1}{L_1 - LP_1} \cdot \left(\frac{e^{P_1 - L_1/L} - 1}{e^{P_1} - 1}\right) - \frac{LP_2}{L_2 - LP_2} \cdot \left(e^{L_2/L} \frac{e^{P_2 - L_2/L} - 1}{e^{P_2} - 1}\right)$$

$$F_b = \frac{LP_1}{L_1 + LP_1} \cdot \left(\frac{e^{P_1 + L_1/L} - 1}{e^{P_1} - 1}\right) - \frac{LP_2}{L_2 + LP_2} \cdot \left(e^{-L_2/L} \frac{e^{P_2 + L_2/L} - 1}{e^{P_2} - 1}\right)$$

$$F_c = \frac{L_2}{LP_2} \cdot \left(1 - \frac{P_2}{e^{P_2} - 1}\right) - \frac{L_1}{LP_1} \cdot \left(1 - \frac{-P_1}{e^{-P_1} - 1}\right)$$

Appendix C

Analytical model for numerical instabilities caused by non-local effects

Numerical instabilities caused by the coupling of the time-independent neutral-modelling to the explicit time-dependent plasma simulation have been observed in the SAFE-code calculations. They can be explained solving a simplified 1D-model equation for the plasma temperature $T = T_i + T_e$ analytically:

$$\dot{T} + (u \cdot T)' = -\frac{2}{3}\frac{(T_0 + \frac{3}{2}T) \cdot S_n}{n} \tag{C.1}$$

This model equation describes the temperature transport along field lines neglecting dissipative effects (heat conduction) and energy fluxes due to velocity changes ($nT \cdot \frac{\partial u}{\partial x}$). The energy losses of the plasma are caused by the interactions with neutral particles. For simplification it is assumed that each reionization process removes an energy of $T_0 + \frac{3}{2}T$ ($T_0 = 15\,eV$) from the plasma.
The neutral flux S_n is determined by the fraction of the plasma flux ($n_t c_s$) reflected at the target (Reflection coefficient R). This flux is instantaneously reionized in a region of length L around point S at a distance d from the target surface (point T):

$$S_n = \frac{R}{L} n_t c_s$$

The differential equation (C.1) is discretized using the 3-point model shown in the figure below.

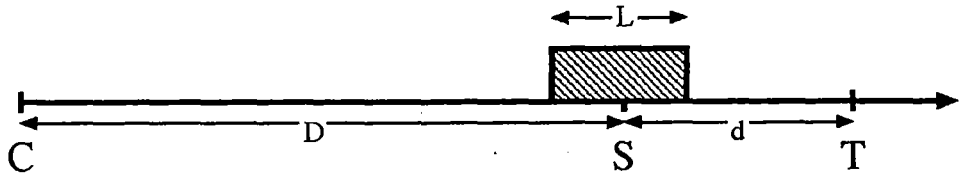

Boundary conditions:
The core temperature T_c – at a distance D from the reionization region – is prescribed and at the target the flow velocity is set to $u = c_s$ (Bohm-criterion).

The equations for the time evolution of T_s and T_t are derived assuming that the particle flux-balance is fulfilled so that $n_c u_c = n_s u_s = n_t c_s$. One finds the coupled differential equations:

$$\dot{T}_s = \dot{T}_t + \frac{n_t c_s}{n_s d}\left[\frac{T_c - T_s}{F} - \frac{Rd}{L}(T_v + T_s)\right]$$

$$\dot{T}_t = \frac{n_t c_s}{n_s d}\left[\frac{n_s}{n_t}T_t - T_s\right]$$

with $\quad F = \frac{D}{d}\ ; \quad T_v = \frac{2}{3}T_0.$

The time t is replaced by $t' = \frac{t}{\tau}$ where $\tau = \frac{n_t c_s}{n_s d}$ is the typical time for pressure transport from point S (reionization zone) to point T (target).

Characteristic features of the differential equations:

- The equations have no stationary solution ($\frac{\partial T_s}{\partial t'} = \frac{\partial T_t}{\partial t'} = 0$) if the energy losses $\frac{Rd}{L}(T_v + T_s)$ around point S are larger than the energy flux $\frac{T_c - T_s}{F}$ into the reionization zone.
- A purely exponential decay of T_s and T_t in time is found if $\left(1 - \frac{n_s}{n_t} - \frac{1}{F} - \frac{Rd}{L}\right)^2 \geq 4 \cdot \frac{n_s}{n_t}\left(\frac{1}{F} + \frac{Rd}{L}\right)$
- Oscillations of the solutions in time occur for $\left(1 - \frac{n_s}{n_t} - \frac{1}{F} - \frac{Rd}{L}\right)^2 < 4 \cdot \frac{n_s}{n_t}\left(\frac{1}{F} + \frac{Rd}{L}\right)$

Especially for the TEXTOR-calculations with the pumplimiter ALT II the various factors can be estimated assuming that the reionization takes place underneath the blades:

$R \approx 0.6$
$\frac{d}{L} \approx 1$
$\frac{n_s}{n_t} \approx 2$
$F \approx 7$
$T_c \approx 100eV$

Using these values one finds that a stationary solution exists but that the explicit time-marching scheme ($\tau \ll 1$) creates oscillations even in T_s.

To study this instability one has to look in detail into the solutions for T_s and T_t :

$$T_s(t') = e^{\frac{1-f-r}{2}\cdot t'} \cdot \left\{ \frac{A}{W} \cdot sin(\frac{W}{2} \cdot t') + B \cdot cos(\frac{W}{2} \cdot t') \right\} + \frac{G}{r}$$

$$T_t(t') = e^{\frac{1-f-r}{2}\cdot t'} \cdot \left\{ \frac{C}{W} \cdot sin(\frac{W}{2} \cdot t') + D \cdot cos(\frac{W}{2} \cdot t') \right\} + \frac{G}{r}$$

with

$$\begin{aligned}
f &= \tfrac{n_s}{n_t} \\
r &= \tfrac{1}{F} + \tfrac{Rd}{L} \\
W &= \sqrt{4 \cdot fr - (1-f-r)^2} \\
G &= \tfrac{T_c}{F} - \tfrac{Rd}{L} \cdot T_v \\
A &= T_s(0) \cdot (1+f-r) + \tfrac{G}{r}(1-f+r) - 2f \cdot T_t(0) \\
B &= T_s(0) - \tfrac{G}{r} \\
C &= 2f \cdot T_s(0) - \tfrac{G}{r}(1-f+r) - T_p(0) \cdot (1+f-r) \\
D &= T_t(0) - \tfrac{G}{r}
\end{aligned}$$

The functions $T_s(t')$ and $T_t(t')$ have been calculated for the TEXTOR-case with the initial values $T_s(0) = 15eV$ and $T_t(0) = 10eV$. The result elucidates that before information can reach the target surface ($t' \leq 1$) the temperature in the reionization zone has dropped below zero while the target temperature is nearly unaffected and shows a smooth exponential decay.

Bibliography

[1] TH. PÜTZ:
Entwicklung eines Finite Elemente Verfahrens zur Modellierung der Plasmaströmung in der Randschicht von TOKAMAKS
Berichte des Forschungszentrums Jülich **JÜL 2942**, Jülich (1994)

[2] M. BAELMANS:
Code Improvements and Applications of a Two-dimensional Edge Plasma Model for Toroidal Devices
Berichte des Forschungszentrums Jülich **JÜL 2891**, Jülich (1994)

[3] S.I. BRAGINSKIJ:
Review of Plasma Physics **1**, 205
Ed. M.A. Leontovich, Consultants Bureau, New York (1965)

[4] S.V. PATANKAR:
Numerical Heat Transfer and Fluid Flow
Hemisphere Publishing Corportation, New York (1980)

[5] B.J. BRAAMS:
Dissertation, The State University at Utrecht,
The Netherlands (1986)

[6] TH. PÜTZ, D. REITER, M.W. WUTTKE:
Contributions to Plasma Physics **34 2/3** (1994), 404 - 409

[7] T.D. ROGLIEN, J.L. MILOVICH, M.E. RENSINK, AND G.D. PORTER:
Journal of Nuclear Materials **196-198** (1992), 347

[8] R. LÖHNER, K. MORGAN, O.C. ZIENKIEWICZ:
Computer Methods in Applied Mechanics and Engineering **51** (1985), 441

[9] L.C. DUTTO:
Application of GMRES Algorithm to solve the compressible Navier-Stokes equations, **INRIA - 1234**, (1990)

[10] A.J. BAKER, J.W. KIM:
International Journal for Numerical Methods in Fluids **7** (1987), 489

[11] TH. PÜTZ, A. KALECK, D. REITER, M.W. WUTTKE, P. BÖRNER:
Europhysics Conference Abstracts **18B / Part II** (1994), 758-761

[12] P.C. STANGEBY, G.P. MADDISON:
Europhysics Conference Abstracts **18B / Part II** (1994), 906-909

[13] D. REITER:
Journal of Nuclear Materials **196-198** (1992), 80

[14] R.K. JANEV ET AL.:
Springer Series on Atoms and Plasmas **4** (1987)

[15] J. NEUHAUSER ET AL.:
Europhysics Conference Abstracts **18B / Part II** (1994), 706-709

[16] R. ZANINO: *Journal of Nuclear Fusion* **196-198** (1992), 326

[17] A. RONZHEIMER: *DFVLR-FB* **88-34** (1988), 22

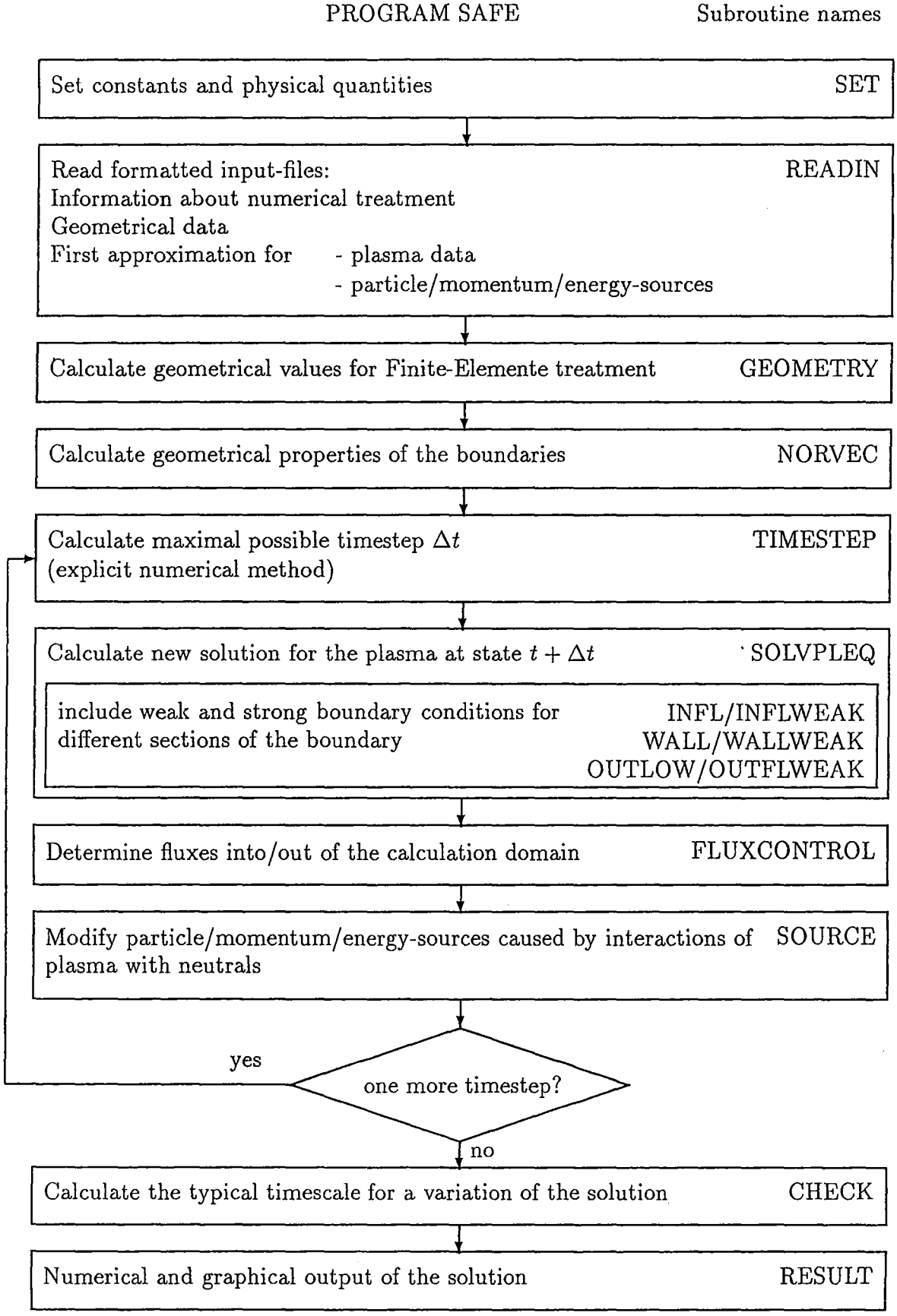
PROGRAM SAFE
Subroutine names
Set constants and physical quantities
SET
Read formatted input-files:
Information about numerical treatment
Geometrical data
First approximation for - plasma data
- particle/momentum/energy-sources
READIN
Calculate geometrical values for Finite-Elemente treatment
GEOMETRY
Calculate geometrical properties of the boundaries
NORVEC
Calculate maximal possible timestep Δt
(explicit numerical method)
TIMESTEP
Calculate new solution for the plasma at state $t + \Delta t$
SOLVPLEQ
include weak and strong boundary conditions for different sections of the boundary
INFL/INFLWEAK
WALL/WALLWEAK
OUTLOW/OUTFLWEAK
Determine fluxes into/out of the calculation domain
FLUXCONTROL
Modify particle/momentum/energy-sources caused by interactions of plasma with neutrals
SOURCE
one more timestep?
yes
no
Calculate the typical timescale for a variation of the solution
CHECK
Numerical and graphical output of the solution
RESULT

SUBROUTINE SOLVPLEQ

IONS:

1. Integrate the variables (density, momentum, energy) over each element

2. Predict a new solution at time $t + \frac{\Delta t}{2}$ for the dissipation free transport equations

3. Modify ion-pressure and -temperature according to this new solution

4. Consider the weak boundary-conditions at different sections of the boundary (inflow, outflow, walls)

5. Calculate a solution after timestep Δt using the modified values after the steps (1.-4.) including dissipation effects

6. Set strong boundary-conditions

ELECTRONS:

Solve the nonlinear heat-conduction-equation implicitely for the timestep Δt (including the boundary-conditions)

THE SAFE-CODE

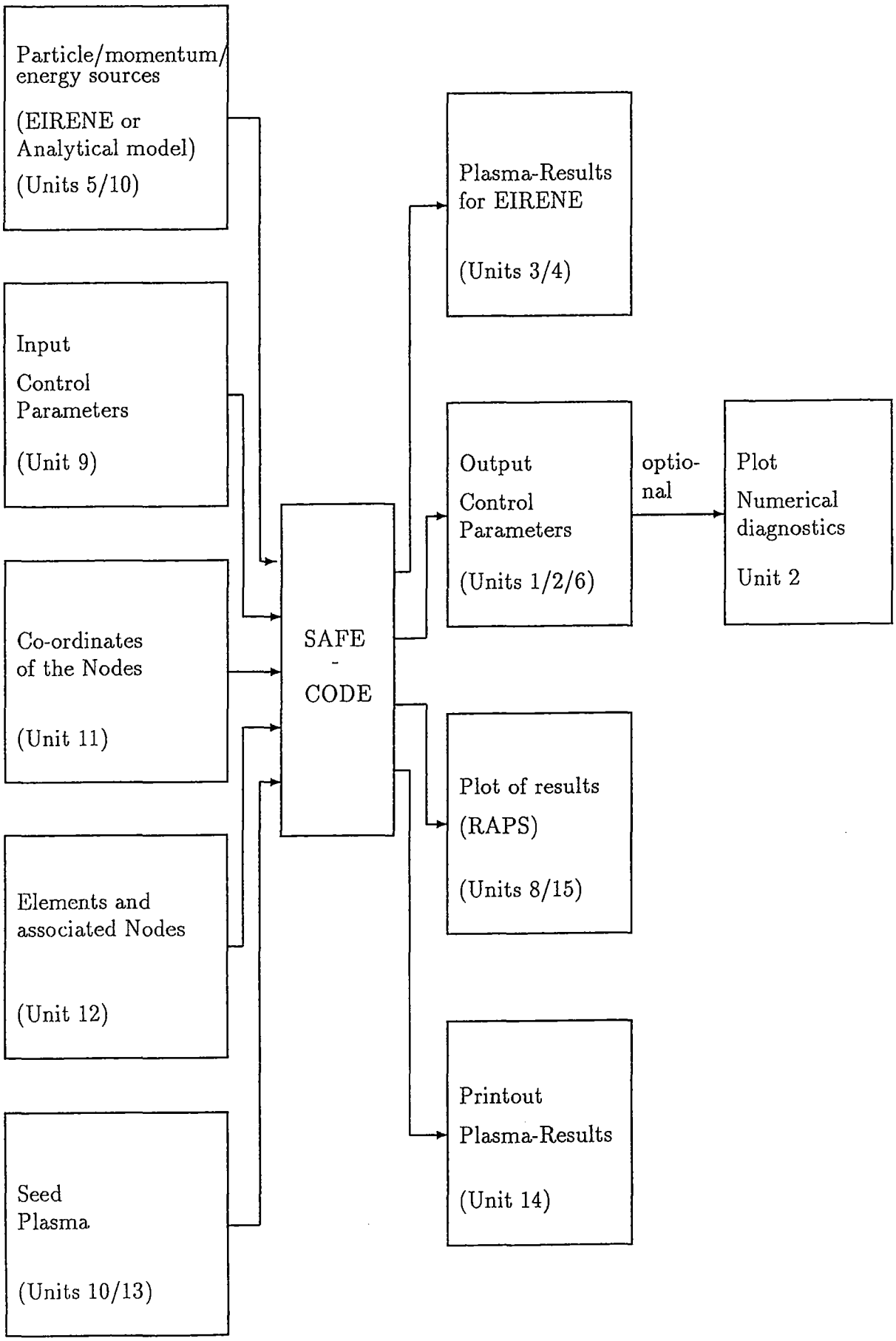

FORSCHUNGSZENTRUM JÜLICH GmbH

KFA

Jül-3220
April 1996
ISSN 0944-2952